POLITECNICO DI TORINO

Master of Science in Automotive Engineering

Master's degree thesis

Model-based optimization of the calibration through Design of Experiments in a diesel engine running with conventional fuel and HVO

Academic supervisor

Prof. Stefano D'Ambrosio

Assistant supervisor

Prof. Roberto Finesso

Dott. Alessandro Mancarella

Ing. Andrea Manelli

Candidate

Davide Apa

Academic year 2021-2022

Abstract

The aim of this thesis is to perform the optimization of the calibration for the F1A diesel engine for different fuels (diesel B7 EN590 and HVO) in a regime of convectional compressed ignition CI combustion. The main investigated outputs are the pollutants (NOx, soot, HC, CO), BSFC and combustion noise CN. The optimization was carried out on the base of Design of Experiments DoE that include statistical techniques aimed at the design and development of controlled tests and subsequent modelling based on their results. Starting from the creation of variation list of experiments based on non-factorial techniques proceeding with data collection and screening to finally arrive to the model fitting and validation till the optimization on the base of prefixed performance goals. In doing so the capabilities of ETAS ASCMO will be compared to the ones of the MATLAB specific toolboxes MBC and CAGE and the applied methodologies described. The optimized points obtained from both the software were compared by testing them in the test cell, to understand which of the two modelling and optimization methods gives results closer to those obtained during the tests.

Contents

List of Tables ..... **IV**
List of Figures ..... **V**
1. Introduction **1**
2. CI engine combustion model, emissions and CN combustion noise **3**
2.1 Heat release rate HRR 3
2.1.1 Ignition delay 4
2.1.2 Premixed combustion 4
2.1.3 Mixing controlled 4
2.1.4 Late combustion 4
2.2 Conceptual model of combustion in CI engine 4
2.3 NO_x formation 6
2.3.1 The thermal mechanism 6
2.3.2 Prompt mechanism 7
2.3.3 NO_2 formation 7
2.4 PM formation 8
2.5 CO formation 8
2.6 HC emissions 9
2.7 Diesel combustion noise 9
3. CI engine fuels characteristics **11**
3.1 Diesel fuel features 11
3.2 Biodiesel features 11
3.3 HVO 12
4. Design of Experiments **13**
4.1 DoE introduction 13
4.2 Space filling DoE 14
4.3 Optimal DoE 14
5. Regression model, its improving and adequacy check **16**
5.1 Linear regression model 16
5.2 Gaussian Process regression 17
5.3 Statistical indicators 17
5.3.1 Residuals 17
5.3.2 Coefficient of determination R^2 18
5.3.3 R^2_{adj} adjusted coefficient of determination 18
5.3.4 RMSE Root mean square error 18
5.3.5 PRESS Prediction error sum of squares statistic 19
5.4 Outliers detection 19

5.5 Transformation 20
6. Experimental set-up 21
6.1 Engine 21
6.2 Dynamometer 22
6.3 Engine cooling system 23
6.4 Fuel metering system 23
6.5 Sensors 23
6.5.1 Pressure sensors 23
6.5.2 Temperature sensors 24
6.6 Emissions measurement systems 24
6.6.1 CO and CO_2 measurement 24
6.6.2 NO and NOx measurement 25
6.6.3 HC measurement 26
6.6.4 O_2 measurement 26
6.6.5 PM measurement 27
7. Modelling 28
7.1 Preliminary tests 28
7.2 DoE creation 30
7.3 MBC procedure for model fitting 32
7.3.1 1250x36 35
7.3.2 2000x163 37
7.3.3 2250x274 39
7.4 ASCMO procedure for model fitting 41
7.4.1 1250x36 43
7.4.2 2000x163 45
7.4.3 2250x274 47
7.5 Optimization results 49
7.5.1 Results comparison 50
8. Conclusions 55
References 56

List of Tables

Table 2.1- Rate constant for NO formation [3]. 7
Table 4.1 - Optimality criteria description. 15
Table 5.1 - Typical value of scaling factor λ. 20
Table 6.1 - Description of the software compartment used in test procedure. 21
Table 6.2 - Technical characteristics of the engine. 21
Table 6.3 - Pressure sensors technical data [18]. 24
Table 7.1 - Working points inputs variation range 29
Table 7.2 – Statistical indicators polynomial model MBC 1250x36 diesel. 35
Table 7.3 - Statistical indicators polynomial model MBC 1250x36 HVO. 36
Table 7.4 - Statistical indicators polynomial model MBC 200x163 diesel. 37
Table 7.5 - Statistical indicators polynomial model MBC 200x163 HVO 38
Table 7.6 – Statistical indicators polynomial model MBC 2250x274 diesel. 39
Table 7.7 - Statistical indicators polynomial model MBC 2250x274 HVO. 40
Table 7.8 - Statistical indicators GP model ASCMO 1250x36 diesel. 43
Table 7.9 - Statistical indicators GP model ASCMO 1250x36 HVO. 44
Table 7.10 - Statistical indicators GP model ASCMO 2000x163 diesel. 45
Table 7.11- Statistical indicators GP model ASCMO 2000x163 HVO. 46
Table 7.12 - Statistical indicators GP model ASCMO 2250x163 diesel 47
Table 7.13- Statistical indicators GP model ASCMO 2250x163 HVO. 48
Table 7.14 - 1250x36 optimization criterion and constraints 49
Table 7.15 – 2000x163 optimization criterion and constraints 49
Table 7.16 – 2250x274 optimization criterion and constraints 50

List of Figures

Figure 1.1 - Engine map coverage WLTP vs RDE. 1
Figure 1.2 - Back box model scheme. 1
Figure 2.1- HRR [3]. 3
Figure 2.2 - Schematic of diesel combustion evolution for a representative operating point [4]. 5
Figure 2.3 - Steady phase combustion process [4]. 6
Figure 2.4 - NO_2 as percent of total NO_x in diesel exhaust as function of load and speed [3]. 7
Figure 2.5 - Soot production process development in time [3]. 8
Figure 2.6 - Typical trend of spectrum frequency of the pressure [1]. 10
Figure 4.1 - OFAT method vs DoE. Example of design of space of 2 parameters process with iso-efficiency zones. 13
Figure 4.2 - Space filling examples with 2 factors sampling: Sobol sequence on the left and Latin hypercube sampling on the right. 14
Figure 5.1- Example of outlier. 19
Figure 6.1- Engine layout and cooling system. 22
Figure 6.2 - AVL APA 100 [17]. 22
Figure 6.3 - NDIR scheme [19]. 25
Figure 6.4 - chemiluminescence detector CLD schematic diagram [20]. 25
Figure 6.5 - FID layout [19]. 26
Figure 6.6 - POD layout [19]. 27
Figure 6.7 - Smoke meter scheme [22]. 27
Figure 7.1- Procedure workflow 28
Figure 7.2 - 1250x36 LP EGR and HP EGR valve actuation constraints. 29
Figure 7.3 - 2000x163 LP EGR and HP EGR valve actuation constraints. 30
Figure 7.4 - 2250x274 LP EGR and HP EGR valve actuation constraints. 30
Figure 7.5 - Selection of the number of input of the DoE on left and regression model selection on right side. 31
Figure 7.6 - Selection of the optimal criteria DoE number of points on the left, selection of input levels on the right. 31
Figure 7.7 - Definition of the constraint on HP EGR and LP EGR. 32
Figure 7.8 – Model test plan. 33
Figure 7.9– Procedure of model improvement [24]. 33
Figure 7.10 – PEV surface view. 34
Figure 7.11 - Response polynomial model MBC 1250x36 diesel. 35
Figure 7.12 – Response polynomial model MBC 1250x36 HVO. 36
Figure 7.13 – Ressponse polynomial model MBC 2000x163 diesel. 37
Figure 7.14 – Ressponse polynomial model MBC 2000x163 diesel. 38
Figure 7.15 - Ressponse polynomial model MBC 2250x274 diesel. 39
Figure 7.16 - Ressponse polynomial model MBC 2250x274 HVO. 40
Figure 7.17 – Input and output selection ASCMO. 41
Figure 7.18 – LOO leave one out average RMSE vs model training data set size. 41
Figure 7.19 – Measured vs predicted graph. 42
Figure 7.20 – Studentized residuals vs predicted graph. 42
Figure 7.21 - Ressponse GP model ASCMO 1250x36 diesel. 43
Figure 7.22 - Ressponse GP model ASCMO 1250x36 HVO. 44
Figure 7.23 - Ressponse GP model ASCMO 2000x163 diesel. 45
Figure 7.24 - Ressponse GP model ASCMO 2000x163 HVO. 46
Figure 7.25 - Ressponse GP model ASCMO 2250x163 diesel. 47
Figure 7.26 - Ressponse GP model ASCMO 2250x163 HVO. 48
Figure 7.27 – 1250x36 diesel optimization number 10 table 7.14 input calibration. 51

Figure 7.28 - – 1250x36 HVO optimization number 10 table 7.14 input calibration. 51
Figure 7.29 - 1250x36 diesel optimization number 10 table 7.14 output results. 51
Figure 7.30 - 1250x36 HVO optimization number 10 table 7.14 output results. 52
Figure 7.31 – optimization number 7 for diesel and number 1 for HVO of table 7.14. 52
Figure 7.32 - optimization number 8 for diesel and number 8 for HVO of table 7.15 52
Figure 7.33 - optimization number 6 for diesel and number 2 for HVO of table 7.16 53
Figure 7.34 - Point 1250 [rpm] x 36 [Nm] optimal calibration for conventional diesel and HVO vs Base diesel calibration 53
Figure 7.35 - Point 2000 [rpm] x 163 [Nm] optimal calibration for conventional diesel and HVO vs Base diesel calibration 54
Figure 7.36 - Point 2250 [rpm] x 274 [Nm] optimal calibration for conventional diesel and HVO vs Base diesel calibration 54

1. Introduction

In the last decades given the growth and development of the wheeled transport sector, commercial and private one, with consequently increase of the pollutant emissions directly related to the usage of vehicle, the international legislation emission limits and test procedure have become more stringent and challenging for car manufacturer. The upcoming introduction of RDE real drive emissions, which is meant to further expand the operating range of the engine during test with respect the WLTP (world-wide harmonized light duty test procedure), by introducing random cycle based on different environmental and driving condition [1]. Parallel to this, research has led to the introduction and development of new fuels so-called biofuels which are promising to accelerate the reduction of pollutants emitted by vehicles. Unfortunately, they need to be further studied and tested before being able to represent a substitute to petroleum-derived fuels so that no additional technologies will be introduced to internal combustion engines already developed today, which would bring additional costs to the OEMs. For these reasons the car manufacturers are constrained to create robust calibration of the actuators and systems of the powertrain to face the regulated emissions limits. Figure 1.1 shows the difference in a qualitative way between RDE and WLTP concerning engine map coverage.

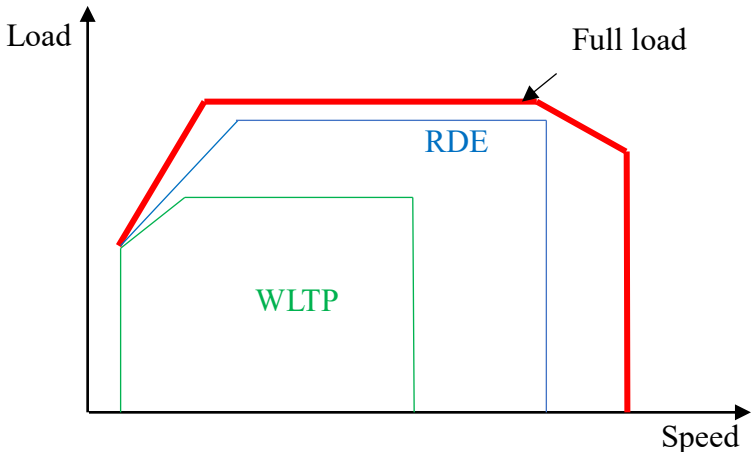

Figure 1.1 - Engine map coverage WLTP vs RDE.

The number of variables to be controlled is high due the complexity of modern engine, so studying all possible combination of parameters during the preliminary phase of engine calibration is costly and more over unfeasible on time base, is mandatory to lean on model-based calibration. The model can be physical (white box model), empirical (black box model) or a hybrid version between these two types (grey box model). The physical model takes into account all the chemical reaction and physical processes presents during the combustion development in the combustion chamber. However, this kind of approach since is based on CFD analysis needs high computational power so very difficult to obtain real time capability.

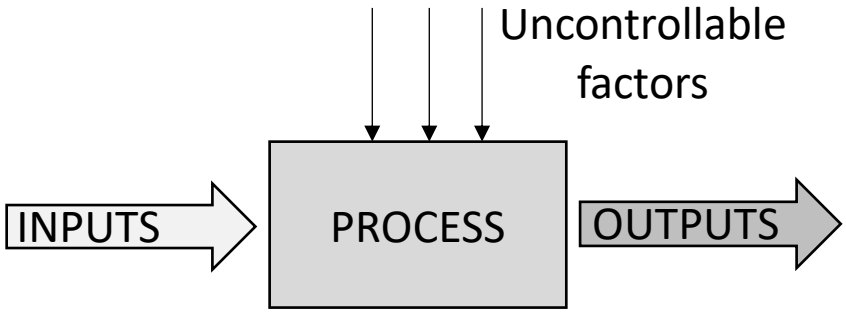

Figure 1.2 - Back box model scheme.

In such scenario the trend to use of non-physical empirical models has spread, studies revealed that model-based calibration assisted by modelling and DoE Design of Experiments application is adequate for calibrating [2]. This kind of models, figure 2, take into consideration the observed system operation under well-defined inputs. DOE implementation guarantees in advance to sets the most influential inputs during the experimental process, in order to identify the empirical mathematical models from the observed results (outputs). The optimization of the calibration, also in case that the engine under test complies with the regulations, can improve the pollutant emissions upstream the aftertreatment system used. A clear consequence of this is the decrease of workload that the aftertreatment system has to bear, limiting its performance decay over time. For instance, the required interval between self-regenerations of the particulate filter can be lengthened thus benefitting from a reduction in fuel consumption.

2. CI engine combustion model, emissions and CN combustion noise

In this chapter will be discussed the combustion model of and the relative pollutant emissions the combustion process can be subdivided in sequences. The first step is the injection of fuel through the nozzle. Injected fuel when it comes into contact with the hot air at high pressure, environment created during the compression stroke, is atomized into small drops, which begin to evaporate. Vaporized fuel mix with air until the mixture has reached the autoignition point. This premixed combusted fuel portion compresses ad heats up the unburned mixture that is just formed, helping it to reach the autoignition before and speed up the vaporization of the fuel that is still liquid. Injection ends when the desired amount of fuel has entered in the combustion chamber. Premixed combustion is a quick process that exploits only a part of the calorific power of the fuels, the rest of the heat is released depending on the rate at which the air mixes with the burned and burning fuel fraction. This phase is called diffusion flames since the "fuel and the air diffuse into each other and react" [3]. When the whole combustion process is ended all the fuel has passed into the afore mentioned phases.

2.1 Heat release rate HRR

To better identify and characterize each of the combustion phases is worth to take consideration the analysis of the HRR. The HRR gives information on the combustion process development on the base of the in-cylinder p pressure trend in function of the θ crank angle p(θ). The HRR expressions represents the first law of thermodynamics applied to an open system in which the only mass that is added is the fuel mass injected.

$$\frac{dQ}{dt} - p\frac{dV}{dt} + m_f h_f = \frac{dU}{dt} \tag{2.1}$$

In which e the first term starting from the left is the heat transfer the second is the work done by the system while m_f and h_f are respectively the mass of fuel injected and its enthalpy U is the internal energy of the components inside the system. The equation 2.1 becomes equal to the 2.2 assuming that both enthalpy and internal energy are sensible and the components inside the cylinder are ideal gases.

$$\frac{dQ}{dt} = \frac{k}{k-1}p\frac{dV}{dt} + \frac{1}{k+1}V\frac{dp}{dt} \tag{2.2}$$

Where k is the ratio of the specific heat at constant pressure and constant volume. In figure 2.1 are reported the different phases of the combustion process in a CI engine.

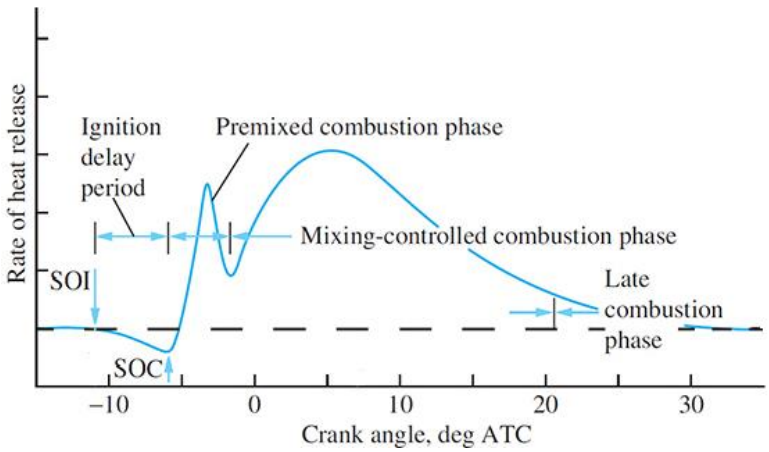

Figure 2.1- HRR [3].

2.1.1 Ignition delay

The ignition delay phase starts as soon as the fuel is injected in the combustion chamber, so it begins the start of injection SOI and finishes at the start of combustion SOC. As can be seen in figure 2.1 the slope of the HRR is negative in this phase this is due to the heat absorbed by the fuel to evaporates and the heat loss through the wall chamber. The ignition delay is affected by both physical and chemical phenomenon. The physical ones are related to the time it takes for the fuel to atomize, evaporate and consequently mix with air. Chemical one instead involves all the mechanisms that concern break of the branches of the hydrocarbon chains to simpler molecules. The ignition as said ends at the SOC which is conceptually placed in the point where the HRR has an inversion of the slope.

2.1.2 Premixed combustion

Premixed combustion is the phase that start as soon as ignition delay finishes. In this phase the rich air fuel mixture burns quickly causing a peak of the HRR in a few crank angles. This peak of HRR is strictly related to the ignition delay since the longer it is the more the quantity of fuel accumulated can mix and burns all at the same time.

2.1.3 Mixing controlled

In this phase the majority of the fuel chemical energy is released. This phase is mainly dependent on the rate at which fuel vapour mix with air so at the rate at which the fuel is available for combustion during the injection.

2.1.4 Late combustion

The combustion develops also in the expansion stroke. The main reasons are that in this phase the product of the previous one still contains low residual chemical energy that can be released. The Complete combustion is achieved but the rate at which this occurs begins to decay as temperature drops due to the expansion.

2.2 Conceptual model of combustion in CI engine

The conceptual model developed on the base of optical analysis of the combustion process in [4] gives a basic scheme of the evolution of the previous mentioned phases in case of a typical diesel engine combustion. The work carried by these studies give the insight of the principle mechanism for soot and NO_x formation. In figure 2.2 is represented the schematic evolution of the process in a representative operating condition, from the start of injection through the early part of the mixing-controlled burn [4]. This time development can be affected in non-experimental condition by the presence of swirl, multiple injections or various boost level. In the early phase of the injection the liquid fuel penetrates in the combustion chamber in form of a spray composed by drops, the hot air entrained between the droplets causes their evaporations. The fuel continues to penetrates and start to slow down while the vapour sheet starts growing around the liquid phase. At around 3 crank angle degrees after start of injection ASI the first chemical reactions take places resulting in a faint light emission. Chemical reactions take places in the chemiluminescent region, this region, that is rich a region, is featured by a fuel vapour-air equivalence ratio between 2 and 4.

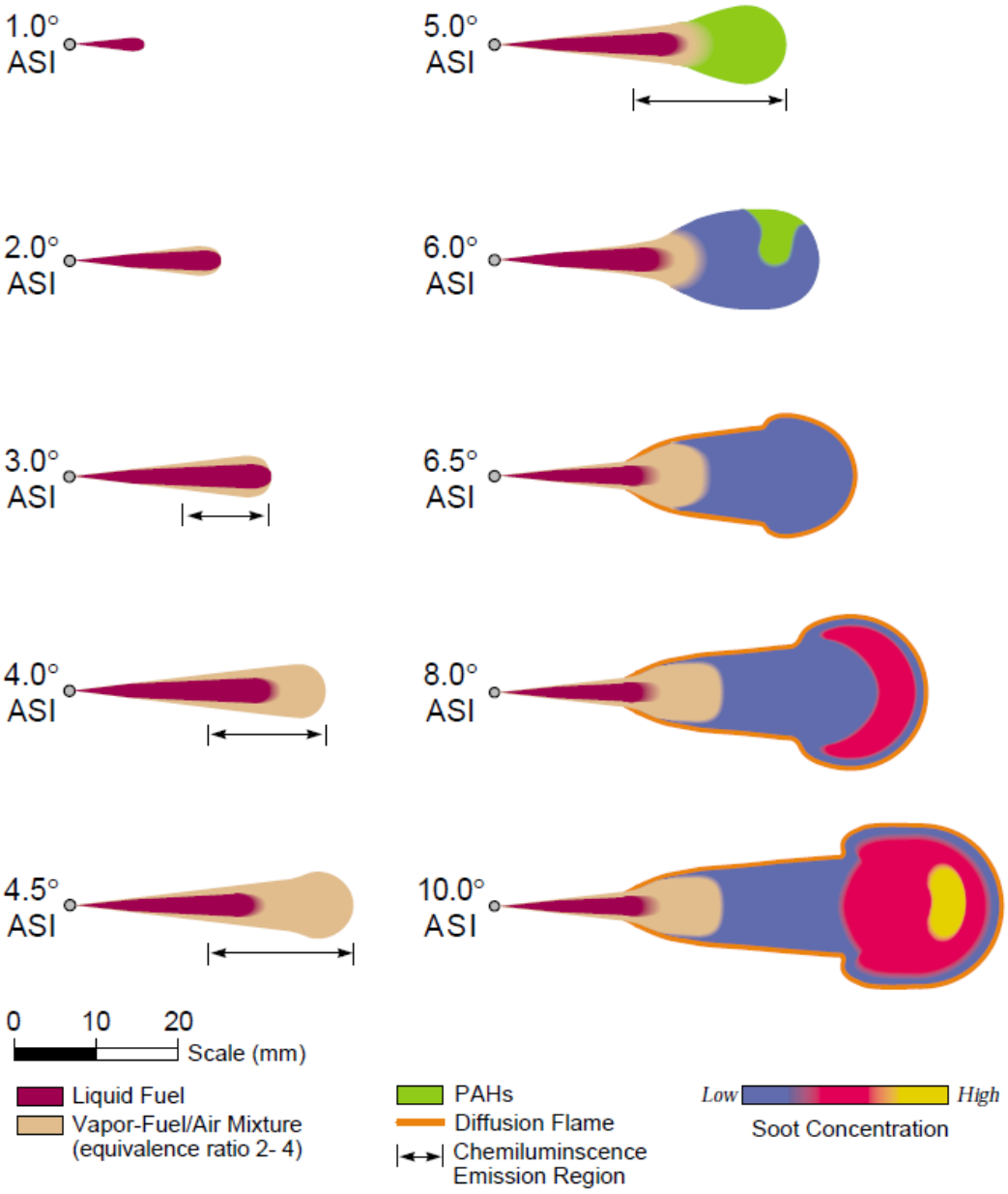

Figure 2.2 - Schematic of diesel combustion evolution for a representative operating point [4].

At 4.5° ASI is where conceptually the premixed combustion start because the chemiluminescence phenomenon is spread all along the leading edges of the plume and the pressure has rapid increase. the formation of PAHs Polycyclic aromatic hydrocarbons starts. A diffusion flame is formed around the fuel rich region and the product of the premixed combustion, the PAHs grow and soot start to form. At 6,5° ASI the diffusion flames have surrounded the plume ad the mixing-controlled process starts. The liquid fuel spray is shortened because the heat diffuses by the fin sheet diffusion flames. Diffusion flame is feed by the partially burned fuel particles, entrained air coming from outside the plume, the PAHs and the soot [3]. Since the entire process is affected by turbulence phenomenon the soot formed tends to travel along the vortex in the tip of the plume, here the soot concentration and the dimensions of the particles grow. Near the end of the fuel injection at 10° ASI a thin layer of soot is detected behind the diffusion flame, here the soot formation is promoted by the high temperature reached, even though the major concentration of soot remains in the head vortex where are also located the soot particles of bigger dimensions, probably due to the high residence time of the soot in the region. When the mixed controlled combustion is in steady phase figure 2.3 the temperature in the oxidation

layer grows this is the main cause of the of NO_x in diesel combustion. In this phase can be noticed how the soot is in principle formed at the edge of the fuel rich zone, this observation can explain the presence in the middle of the plume, the blue coloured region in figure 2.3, of soot in the last phases described since the diffusion flame do not produce it directly but on the contrary is responsible of its oxidation. So, by means of the study of steady phase, the presence of a standing premixed flame combined to the one at the start of the combustion process implies that "all the fuel (both for the premixed and mixing-controlled burn) first undergoes fuel-rich premixed combustion and later diffusion-flame combustion" [4, p.26].

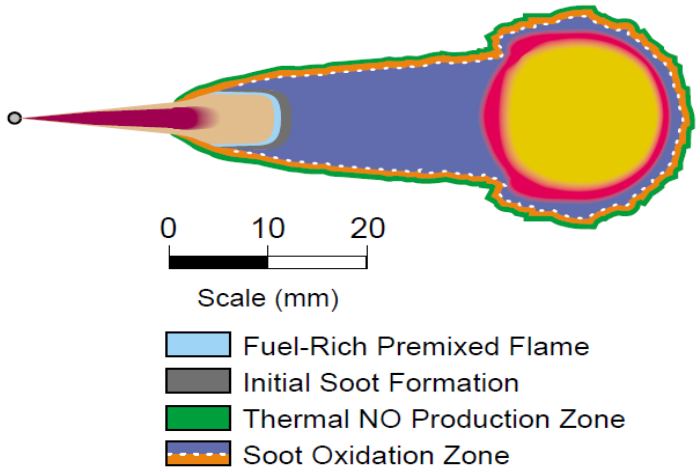

Figure 2.3 - Steady phase combustion process [4].

2.3 NO_x formation

The nitrogen oxides in the diesel engine are composed usually by 70%-90% of NO and 30%-10% of NO_2 [1]. The NO formation is based on mechanism the thermal mechanism and the prompt mechanism, while NO_2 is formed directly from NO.

2.3.1 The thermal mechanism

The thermal mechanism is also known as extended Zeldovich mechanism. This mechanism is based on the kinetics of three main chemical reaction. These reactions are:

$$O + N_2 \leftrightarrow NO + N \tag{2.3}$$

$$N + O_2 \leftrightarrow NO + O \tag{2.4}$$

$$N + OH \leftrightarrow NO + H \tag{2.5}$$

N is provided by the atmospheric air the thermal mechanism is the most relevant at high temperature. The rate constant for forward reactions (2.3), (2.4) and (2.5) and theirs backward rate constant are reported in table 2.1. The first forward reaction and the second and third reverse reaction have high reaction activation energy showing their sensitivity to temperature. This high temperature dependency means also that when the temperature decreases fast as in the expansion stroke the NO concentration freeze due to the high reaction energy needed for backward reactions. This temperature dependency on temperature the process of NO

formation is referred as kinetic process [5], showing higher concentration than the one expected in case of reactions equilibrium.

Reaction	Rate constant, $cm^3/mol \cdot s$	Temperature range, K	Uncertainty, factor of or %
$N_2 + O \rightarrow NO + N$	$7.6 \times 10^{13} \exp[-38{,}000/T]$	2000–5000	2
$N + NO \rightarrow N_2 + O$	1.6×10^{13}	300–5000	±20% at 300 K 2 at 2000–5000 K
$N + O_2 \rightarrow NO + O$	$6.4 \times 10^9 \, T \exp[-3150/T]$	300–3000	±30% at 300–1500 K 2 at 3000 K
$O + NO \rightarrow O_2 + N$	$1.5 \times 10^9 \, T \exp[-19{,}500/T]$	1000–3000	±30% at 1000 K 2 at 3000 K
$H + OH \rightarrow NO + H$	4.1×10^{13}	300–2500	±80%
$H + NO \rightarrow OH + N$	$2.0 \times 10^{14} \exp[-23{,}650/T]$	2200–4500	2

Table 2.1- Rate constant for NO formation [3].

2.3.2 Prompt mechanism

The prompt mechanism has relative low reaction energy activation with respect to thermal mechanism so it goes on also at low temperature, but it is related to the formation of CH radical that are only available in case of rich mixture on the base of the reaction (2.6) [5].

$$CH + N_2 \rightarrow HCN + N \tag{2.6}$$

with rate constant equal to $3.12x10^9 \exp\left[-\frac{10.130}{T}\right]$ [m^3/(kmol·s)] [5].

2.3.3 NO_2 formation

NO can be converted in NO_2 following the reaction (2.7), (2.8) and (2.9) these reactions are the most important for the NO_2/NO distribution [5].

$$NO + HO_2 \leftrightarrow NO_2 + OH \tag{2.7}$$

$$NO + OH \leftrightarrow NO_2 + H \tag{2.8}$$

$$NO + O_2 \leftrightarrow NO_2 + O \tag{2.9}$$

These reactions can go back to NO only if the formed NO_2 is not quenched by cooler fluid. The process is consistent with the condition obtained at low load where the value of the ratio NO_2/NO is the highest.

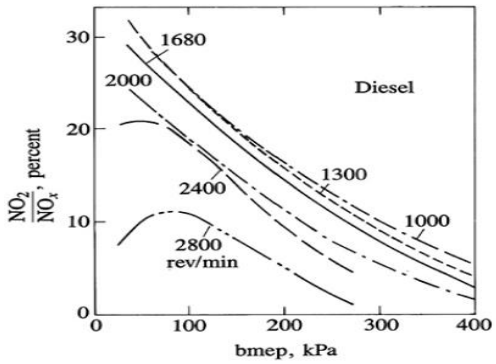

Figure 2.4 - NO_2 as percent of total NO_x in diesel exhaust as function of load and speed [3].

2.4 PM formation

One of the most challenging issue in diesel engine is the emission of particulate matter especially when trade related to NO_x emissions because the condition for reducing one could causes the increase of the other for this reason is we usually speak about trade off. The majority of the CI engine today use direct injection thus combustion develops locally in rich mixture condition, this enhance the PM production. During combustion most of the PM is oxidized but the remaining particles can grow an agglomerate forming corpuscular bodies of irregular shapes and various sizes distributed in the cylinder. The PM has not a fixed chemical composition depending mostly on the operating condition of the engine. The largest amount of this various particle is composed by a combination of carbonaceous product called soot, hydrocarbons and sulphates [5]. The amount of sulphates is related to the percentage of sulphur contained in the fuel that in the last years becomes low circa 10 mg/Kg. The soot is main component of the particulate matter. The soot formation takes place in the fuel rich zone of the spray so where low presence of oxygen does not permit the complete oxidation of fuel. In this zone the partially oxidized fuel fraction is the base block of the soot particle. The main are the PAHs which are the results of partial oxidation and pyrolysis of fuel molecules. When the PAHs start to the dehydrate they join in structure for the van der Walls forces [5] nucleate forming small particle defined of the other of few nanometers called soot Kernels. They are the small amount of the solid part in particulates "the bulk of solid phase material is generated by surface growth" [3, p.669]. Surfaces growth consists in the attachment of the gaseous species on the particles surface. The further growth of the particles happens on the base of agglomeration phenomenon due to collisions. These stages in soot formation can happen at the same time in different zone of the cylinder since the non-homogeneity of the combustion causing a wide distribution in dimesons of the particles. The figure 2.4 shows the evolution in time of the processes in the soot production.

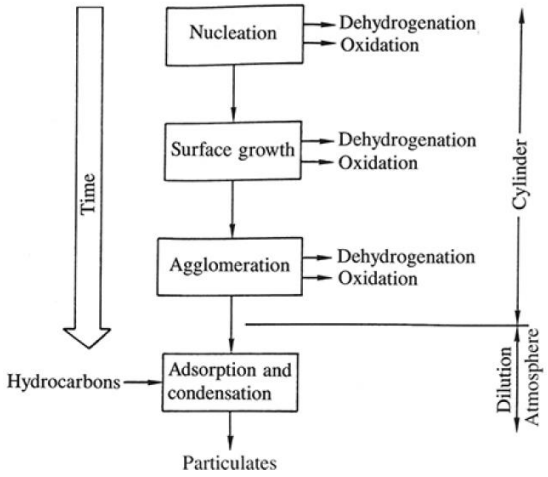

Figure 2.5 - Soot production process development in time [3].

As the depicted in figure 2.4 the last stage take place in the atmospheric environment at the exit of the combustion chamber. The hydrocarbons in the exhaust air condensate and cool entering in contact with air and will be absorbed.

2.5 CO formation

The condition that favours the Co formation is the rich condition so when relative air fuel ratio λ is lower than 1. In CI engine the formed CO is connected to the rich premixed combustion but since the overall λ in the

combustion chamber is way above 1 in all the operating condition the CO can be theoretically all oxidized due to the excess of oxygen. The dominant oxidation reaction in this lean condition is the one of expression 2.10

$$CO + OH \leftrightarrow CO_2 + H \tag{2.10}$$

This reaction is highly dependent on temperature so it slowed during expansion stroke., letting the CO concentration near the value assumed for the reaction equilibrium [5].

2.6 HC emissions

The diesel fuel has a structure composed of various species of hydrocarbons each having different weight and volatility. The complexity of the fuel composition can be increased also during combustion development where part of the fuel is partially oxidized or is pyrolyzed, the range of the molecules complexity expands. The emission of HC is based on two different modalities: the overmixing (over leaning) and the undermixing. The first refers to the condition where the fuel mix with air and the equivalent ratio is minor than 1. The undermixing is due to the presence in the spray of pockets where the high percentage of fuel do not allow complete combustion due to the scarcity in these regions of oxygen. These conditions are strongly dependent on engine load. At idle or low load is more probable that overmixing occurs, while at high load the HC emissions is related to undermixing. The overmixing was recognized as the principle condition for HC emissions [3]. When the fuel is injected into the cylinder, during the ignition delay the fuel on the edges of the spray that goes in lean condition mixture. This mixture formed can be under the lean combustion limit equivalence ratio and does not auto ignite [3]. In this condition the amount of HC emitted is proportional to the quantity of fuel injected during the ignition delay. So, everything that influence the ignition delay such as in cylinder temperature directly affect HC emission. Undermixing can takes place for 2 main reasons. One reason regards the fuel contained in the sac of the injector. The sac is the small volume in the injector tip left filled of fuel in order to stabilize the pressure upstream the injector nozzles. The fuel contained in the sac undergoes to evaporation at the end of the injection event. Due to its low exit velocity it mixes slowly with air during the expansion stroke so in late combustion could escape at the primary combustion and be exhausted [3]. The other causes of undermixing is the overfilling that occurs when the engine operates under fast transient condition.

2.7 Diesel combustion noise

The reduction of engine noise is a fundamental step in the optimization of the comfort level during the operating condition of the vehicle. Combustion noise has source of different nature: mechanical, gas dynamics, combustion noise. The mechanical noise source is related to all the moving mechanical part of the engines that impact during their motion. The impacts cause the engine structure to vibrate that accordingly irradiates the noise. The gas dynamics source includes the vibrating and resonant phenomena related to the gas motion. The main are the motion of the air at the suction and the discharge of the exhaust gasses. The motion in the intake and exhaust manifolds cause the pressure pulses that travel along the manifolds back and foreword causing vibration. The last and most important source is the combustion noise. The combustion noise in CI engine is due to the rapid pressure rise in the cylinder caused by the rapid combustion during the premixed burning phase [1]. To quantify the amount of noise emitted the first step is to analyse the pressure oscillation, since they are periodic, through the application of the Fourier Transform to determine the amplitude of the harmonics with respect of the frequency obtaining the frequency spectrum of the pressure. By analysing the spectrum can be seen as depicted in the figure that at low frequencies the cylinder pressure level depends on the peak pressure reached during the combustion. In the range of the mid frequencies range the harmonics that contribute mainly are the one of the first derivative of the pressure with respect of time (pressure gradient) an

they are the main energy contribution. At high frequencies range the oscillations depend on the vibrations of the gas in the cylinder.

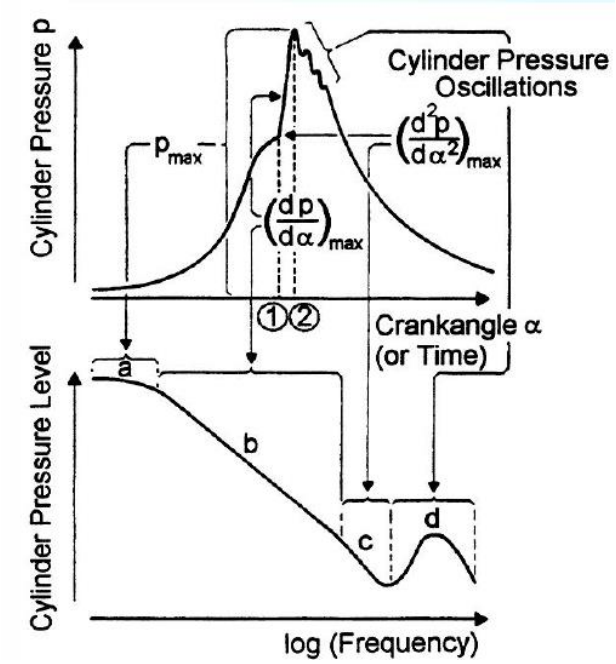

Figure 2.6 - Typical trend of spectrum frequency of the pressure [1].

To get reliable and more precise measure on the base of the pressure signal the transfer function used to compute the response of the engine to such vibrating input is the CAV filter [1]. Other two filters are then applied to the response the A filter and LP filter. The A filter is used to emphasizes the pressure signal at the frequency at which the human ear is sensitive. The LP filter is a low pass filter that cut the oscillation due to combustion chamber resonance that are dependent on its shape and dimensions. As seen what contributes more to combustion noise is the first derivative of the pressure, this high rapid variation of pressure is due to the fast HRR observed in the premixed combustion phase so all the precautions that aim to reduce this gradient are useful. The main adopted is the addition of a pilot injection that is useful to reduce the ignition delay of the main injection. Choosing the optimal fuel quantity of the pilot, the combustion events of both main and pilot become comparable on the base of HRR so smoothing the in-cylinder pressure trend [1].

3. CI engine fuels characteristics

The chapter contains description of the main characteristic of the diesel fuels and their main criticalities, furthermore the HVO properties will be displayed making a parallel between the biodiesel FAME (fatty acid methyl ester) used in the commercial diesel blends on the base of the standard EN 590.

3.1 Diesel fuel features

Diesel fuel is composed by blends of hundreds of different hydrocarbons obtained by the refining the crude oil. The Hydrocarbons present have a molecular structure of the type C_xH_y with number of carbon atoms that range from 9 to 26. Those species can be divided into four groups: paraffins, olefins, naphthenes and aromatics [6]. These chemical species are present in different proportions of these the lowest is belonging to the aromatics group, because during the refinery operation are minimized as they are detrimental to the quality of ignition since they tend to retard it. This side effect must be avoided in diesel fuels because they need to be highly reactive. In diesel fuels blend are also present in minimum quantity, with respect to the hydrocarbons, residual chemical species from the refining process to which is important to pay attention. Specifically, the presence of sulfur causes after the combustion process the formation of products such as sulfuric dioxide SO_2 and sulfate SO_4. These products entering in contact with the water present in atmosphere leads to the formation of sulfuric acid main component of acid rains. Furthermore the presence of sulfuric products can causes the deterioration of the aftertreatment systems since the SO_2 can combine with water molecules in the exhaust forming hydrated sulfuric acid that contributes to particulate matter emissions or causing sulfur poisoning of the LNT, this implies the actuation of desulfating strategies achieved by incrising the exhaust temperature by post injection of fuel [1]. The current legislation EN 590 imposes a sulfur content minor of 10 ppm for the current diesel fuels known as ULSD ultra low diesel sulfur diesel. The low content of sulfur brings drawback in terms of lubrication provided by the fuel itself. This side effect could be attenuated by addiction of specific additives. One method to measure the quality of the diesel fuel is the calculation of the cetane number. The cetane number CN is computed by:

$$\mathrm{CN} = \%\mathrm{cetane} + 0.15 \times \%\mathrm{HMN} \tag{3.1}$$

with %HMN refers to the percentage of Heptamethyl-none in the blend. The cetane number gives an indication of how much a fuel is prone to ignition. The scale of the cetane number range from 15 for poor quality fuel to 100 for high quality. In CI engine is very important to have fuels with high number of cetane, that guarantees the reduction of the ignition delay. The minimum cetane number of the diesel fuel is established by EN 590 standard to be at least 51.

3.2 Biodiesel features

In recent years the usage of biodiesel spread either as a stand-alone fuel or as addition to diesel derived from oil refining. With biodiesel we refer to fuels obtained by transesterification of the triglycerides contained in vegetable oil and animal fat using alcohol, like methanol or ethanol [6,7] obtaining FAME. The production process of the FAME is expansive, the actual advantages of these fuels is that the they can be obtained from the recycling of food and agricultural waste. This implies a reduction in net carbon emissions compared to fossil fuels, because the carbon emitted during combustion was the one used in the growth of the plant and not the one accumulated underground in the form of oil. The cons related to biodiesel are its higher density and viscosity and lower energy content with respect to diesel, thus running engine with blend composed by 100% of biodiesel require modification of the base engine from the point of view of calibration and of injection

system. Due to residual presence of oxygen and water after the production process, the biodiesel tends to degrade in storage. To attenuate the impact of these characteristics the biodiesel is usually blended with conventional diesel. The amount of this blending is established by the EN 590 standard for diesel in Europe, specifically the percentage cannot overcome the 7%, the addition of biodiesel brings advantages to conventional diesel for Regarding lubrication properties, since it is more viscous and cetane number increase.

3.3 HVO

HVO hydrotreated vegetable oil is a renewable diesel. The source from which is obtained are the same of the FAME but instead of using methanol in its production process the esterification is achieved through the use of hydrogen. This process removes the oxygen and guarantees that the fuel does not oxidize during storage. The HVO meets the requirements of the conventional diesel but it has lower density. HVO is fully miscible with conventional diesel so it is not required a limitation for their blending like it is needed for FAME. HVO can be used 100% pure in commercial engine without applying to them modification. Due to its chemical composition characterized by the absence of aromatic and polyaromatics compounds the cetane number with a value that stands at a minimum of 75 is higher than the one of conventional diesel. This implies that the combustion takes place with a high quality.

4. Design of Experiments

In this chapter is discussed in brief the theory behind the DoE, focusing on the two different DoE typologies used in this work: optimal design and space filling design

4.1 DoE introduction

In the experimental research the objective is to performs a certain number of test in order to be able to define the physical properties of the process under study. Usually the experiments are conducted in a way that the operations to establish which are the influential controllable parameters and which are the effect of their combination and at the same time trying to minimize the error on the output due to parameters that are uncontrollable. To get a robust experimentation is essential to test every variation of each parameters with respect to the others involved by applying non-statistical method such as the one factor at time method OFAT. The OFAT can misled the operator in the search of response global optimum giving instead as result a local one. An efficient way to speed up this process is to apply the techniques of the so-called DoE in which a matrix of experimental runs in which the factors are changed simultaneously is created.

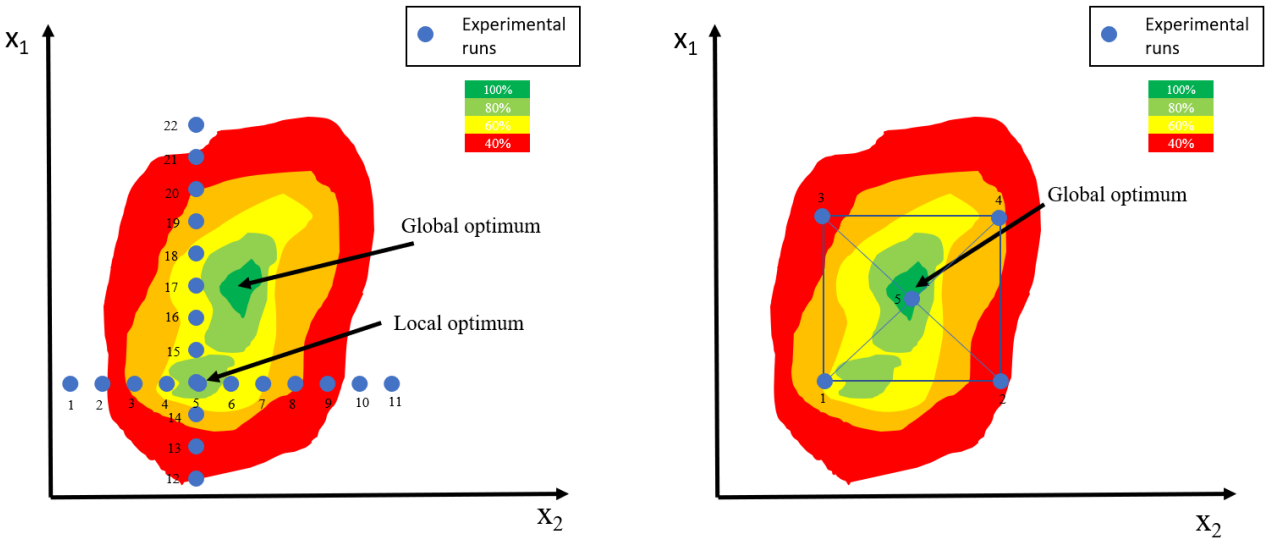

Figure 4.1 - OFAT method vs DoE. Example of design of space of 2 parameters process with iso-efficiency zones.

The main properties of the experimental design are: randomization, replication and blocking, as described in [8]. Randomization means that the runs are conducted randomly. The randomization is based on methods that assign the input of the factors within a set of possible values, this is a way to averaging the influence of non-controllable parameters so eliminate the average bias. Replication consists in the multiple times observation of the experiment for each factor combination (for each time same set of inputs), this assure the estimation of the random error. For blocking is meant the techniques that are used to eliminate the factors that enhance the variability by running the experiments in similar groups. The most commonly used and intuitive designs are the full factorial with n^k trials and fractional factorial n^{k-1}, with n number of levels usually 2 or 3 of the k number of factors [9].

4.2 Space filling DoE

The space filling design spread the trials all over the design space domain uniformly. The cover of all the domain guarantees the ability of the experiment to capture the complexity of the process. The main feature of the space filling design is that it does not need of trials that are located in the central point in the corners of the domain and each point appears only once, hence there is not replication of trails.

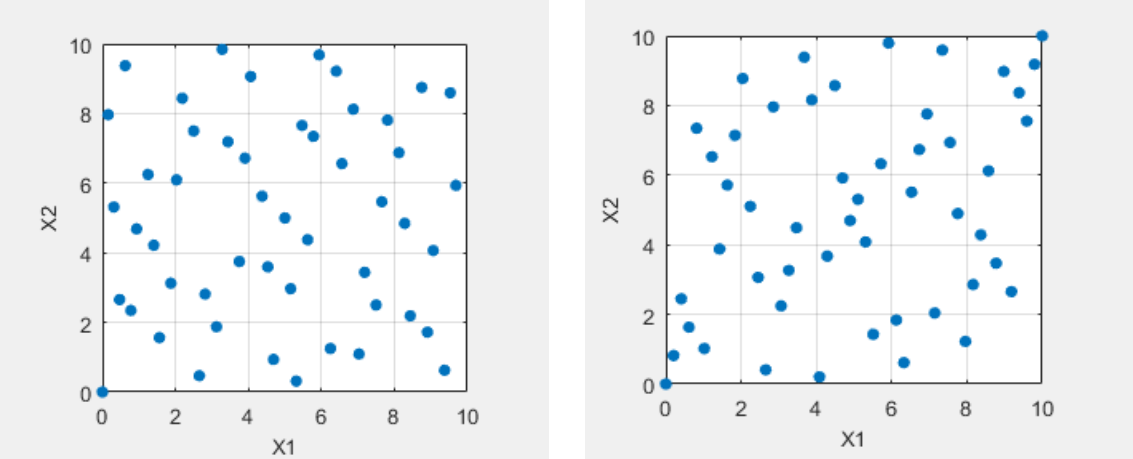

Figure 4.2 - Space filling examples with 2 factors sampling: Sobol sequence on the left and Latin hypercube sampling on the right.

Space filling approach is useful if the designer does not know in advance the process or where it has interesting variation throughout all the region of investigation, do not know the form of the model required for modelling. "Several efficient space filling techniques are based on pseudo random number generators" [10] such as Sobol sequence figure 3.2. The most common space filling method is the Latin-hypercube. In the Latin-hypercube sample method figure 3.2 to compute the set of samples a matrix n×k is constructed and each of its column is composed of a random permutation of the levels, with n number of samples an k factors [8, p.525]. The space filling DoE is particularly suggested to be used in ASCMO.

4.3 Optimal DoE

The optimal design is typically used when the designer has a previous knowledge on the process and knew which the constraints of the response surface are. Optimal design is used if the trials execution is forced to have a reduced number of runs compared to those necessary for factorial design. The optimal design procedure is made up several optimality criteria. Some of them are reported and briefly described in table 3.1.

Optimal design	Optimality criterion
D-optimal	This criterion gives a selection of design points based on the minimization of the confidence region, achieved by maximizing the information matrix [11].
A-optimal	The average variance is minimized, this can be done by minimizing the trace of the inverse of the information matrix [11].

G-optimal	Minimizes the maximum value of the prediction variance in the design region [11].
I-optimal	Focuses on the minimization of the integral, so over the whole design region, of the prediction variance [11].
V-optimal	Set of points in the design region is chosen and their average prediction variance is minimized

Table 4.1 - Optimality criteria description.

In our case study V-optimal design was used to create DoE in MBC. The V-optimal it is suggested in by MATLAB to be the most appropriate method for calibration problem. This optimal method was chosen since a linear regression model was initially chosen due to its simplicity and good ability to predict the path of the required outputs on the basis of previous work carried out by the research team.

5. Regression model, its improving and adequacy check

As afore mentioned the model were created and fitted by means of MATLAB's tool MBC and ETAS ASCMO. For this reason, in this chapter will be given a brief theoretical overview of the regression models used for this project, starting from the simplest one to give a basis on how the models were chosen. Then the main methods to improve the model quality and check its adequacy will be discussed. The actual procedure followed with the both the software is covered in chapter7.

5.1 Linear regression model

Given a data set of observations, if the regressor or independent variable x, is assumed to be related in a linear way to the y, dependent variable or response, the model takes the following structure:

$$y = \beta_0 + \beta_1 x + \varepsilon \tag{5.1}$$

where ε is the random error term assumed to have a mean equal to zero and unknown variance δ^2, β_0 and β_1 are called regression coefficients and are respectively the intercept and the slope. "It is convenient to view the regressor *x* as controlled by the data analyst and measured with negligible error, while the response *y* is a random variable. So, there is a probability distribution for *y* at each possible value for *x"* [12].
The mean of this distribution is:

$$E(y|x) = \beta_0 + \beta_1 x \tag{5.2}$$

and the variance:

$$Var(y|x) = Var(\beta_0 + \beta_1 x + \varepsilon) = \sigma^2 \tag{5.3}$$

Starting from this simple model is possible to create model with multi regressors x, so multi inputs, this kind of model is called multiple regression model and can be described by:

$$y = \beta_0 + \beta_1 x_1 + \beta_2 x_2 \dots \beta_k x_k + \varepsilon \tag{5.4}$$

or if interactions are present

$$y = \beta_0 + \beta_1 x + \beta_2 x_2 + \beta_{12} x_1 x_2 + \varepsilon \tag{5.5}$$

any regression model that is linear in β parameters is a linear regression model regardless of the shape of the surface that it generates. In this case the model is no more represented by a line but a hyperplane in the space of the variables x and y. To determine the regression coefficients the Least squared estimation is used, as described in [13]. Since the relations between the input and output involved in this work, which are non-linear and shows interactions of order greater than 1 the linear model is unable to describe them. One model that guarantees that such behaviour is taken in considerations is the polynomial, this class of model is included in the linear regression thus the general principles of multiple regression can be applied. Polynomial regression models are widely used when the response is curvilinear. The polynomial model of order n is of the form:

$$y = \beta_0 + \beta_1 x + \beta_2 x^2 + \cdots \beta_n x^n + \varepsilon \tag{5.6}$$

The polynomial regression can lead to overfitting over data if the order is too high so it must be carefully selected. Since the process involved in our case study was well known on the base of previous works, the second order was the most suitable choice. The polynomial structure expressed in (5.7) was adopted.

$$y = \beta_0 + \beta_1 x + \beta_2 x^2 + \varepsilon \tag{5.7}$$

and in case of two inputs and interaction the expression (5.7) becomes:

$$y = \beta_0 + \beta_1 x_1 + \beta_2 x_1 + \beta_{11} x^2{}_1 + \beta_{22} x^2{}_2 + \beta_{12} x_1 x_2 + \varepsilon \tag{5.8}$$

5.2 Gaussian Process regression

In the GP Gaussian process is not needed to prior selected or better learn a model but is possible to consider all the infinite models and averaging them. The GP is a non-parametric method. "Non-parametric methods are procedures of statistical inference for models without precise assumptions about the distribution of the sample" [14]. The definition of GP states that:" A Gaussian process is a collection of random variables, any Gaussian process finite number of which have a joint Gaussian distribution" [15, p.13]. Basically, having a data set is possible to make prediction of the output on the base of the average of the most likely line on which the data are supposed to lie. The Gaussian process regression model can be expressed as:

$$f(x) \sim N(m(x), k(x, x')) \tag{5.9}$$

where $f(x)$ is the process output and $m(x)$ is the mean function and k covariance function [15]. The advantage of using GP over the polynomial regression is its straight application, because polynomial regression as afore mentioned needs in advance the selection of base function, furthermore it can be totally specified by its mean and covariance function. The covariance function establishes how similar two inputs x and x' are, therefore how much are similar the function outputs $f(x)$ and $f(x')$. The possibility to choose between different types of Kernel (covariance function) guarantees versatility in the shape that the distribution will have, the most commonly used kernel types will be specified below for more detail about GP refers to [15].

Squared exponential Kernel

The square d exponential Kernel has the following form:

$$k(x, x') = \sigma^2 exp\left(-\frac{r^2}{2l^2}\right) \tag{5.10}$$

σ^2 is the input variance, l is characteristic length scale, this parameter decides how quickly the response can change and therefore influences its smoothness. We will have quickly change of the response so harsh variation for small value of l while the opposite for large one. The r is the distance between the points x and x'.

Matérn Kernel

The Matérn covariance function is defined like this

$$k(x, x') = \frac{2^{1-v}}{\Gamma(v)}\left(\frac{\sqrt{2v}r}{l}\right) K_v\left(\frac{\sqrt{2v}r}{l}\right) \tag{5.11}$$

The term v is a positive parameter $\Gamma(v)$ is the gamma function and K_v is a modified Bessel function [15]. The Matén Kernel is a generalization of the squared exponential. With the variation of the term v is possible to adapt the function variation, a lot of time this kernel works better than the standard Gaussian kernel as it is 'less smooth'.

5.3 Statistical indicators

To check and refine the quality of the model some statistical parameters are taken into considerations. These parameters are based on the study of the differences between the model outputs results and the experimental ones.

5.3.1 Residuals

The residual r_i is computed by means of the difference of the experimental test results and the values obtained by the model:

$$e_i = y_i - \hat{y}_i \tag{5.12}$$

where $\hat{y}_i$ is the i[th] model output and y_i the experimental output. The residuals represent the error between the two evaluations, so if the result is zero the model is perfectly fitted for that observations. This kind of evaluation is too simplistic since the value of e can be off scale with respect the mean value of the process, so is up to the operator to decide the threshold. In order to face this problem is useful to take its value normalized. In particular an operation done in MBC is to take the studentized residuals, that is obtained by dividing e_i by its corrected error variance:

$$r_i = \frac{e_i}{\sqrt{\hat{\sigma}^2\,(1-h_{ii})}} \tag{5.13}$$

where the $\hat{\sigma}^2$is the error variance and h_{ii} is the diagonal term of the hat matrix [13]. The studentized residual is a useful tool to detect outlier as will be discussed in the paragraph 5.4.

5.3.2 Coefficient of determination R^2

This parameter varies in arrange between 0 and 1, it correlates the variation of the data with the correctness of the model. Conceptually it describes how good the model fit the data or better expresses the percentage of point falling on the regression line.

$$R^2 = \frac{SSR}{SST} = 1 - \frac{SSE}{SST} \tag{5.14}$$

Where SSR is the regression sum of square:

$$SSR = \sum_{i=1}^{n}(\hat{y}_i - \bar{y}_i)^2 \tag{5.15}$$

SST is the total sum of squares:

$$SST = \sum_{i=1}^{n}(y_i - \bar{y}_i)^2 \tag{5.16}$$

$\bar{y}_i$ is the mean value of the experimental data, while SSE is the residuals sum of squares:

$$SSE = \sum_{i=1}^{n}(y_i - \hat{y}_i)^2 \tag{5.17}$$

5.3.3 R^2_{adj} adjusted coefficient of determination

R^2 is very sensitive to number of predictors variable, the higher is their number the more its value grows, so it might be affected by the overfitting and gives misleading information about the quality of the model. To deal with this aspect it is worth to compute R^2_{adj}, that takes in consideration the number of the parameters and the number of the data in the sample. Its expression is:

$$R^2_{adj} = 1 - \frac{SSE(n-1)}{SST(n-p)} \tag{5.18}$$

n represents the size of the sample and p the number of regression parameters, this statistical coefficient also allows to compare regressions model with different number of parameters.

5.3.4 RMSE Root mean square error

The root mean square error is useful to quantify the prediction accuracy of the model. As a matter of fact, RMSE measures the difference between values predicted by the model and the one actually observed.

$$RMSE = \sqrt{\frac{\sum_{i=1}^{n}(y_i-\hat{y}_i)^2}{n}} \tag{5.18}$$

5.3.5 PRESS Prediction error sum of squares statistic

The PRESS is an approach used to estimates the consistency of the model. For each data point, the statistic calculates how well the model fits the data point when it is not included in the fit [16].

$$PRESS = \sum_{i=1}^{n}(y_i - \tilde{y}_i)^2 \tag{5.19}$$

The $\tilde{y}_i$ is the model predicted response without the i[th] observation, n is the number of observations. PRESS statistic can be applied to R^2 and RMSE so expression 5.14 and 5.18 become respectively:

$$PRESS\ R^2 = 1 - \frac{PRESS}{SST} \tag{5.20}$$

$$PRESS\ RMSE = \sqrt{\frac{PRESS}{n}} \tag{5.21}$$

5.4 Outliers detection

To improve the quality of the model if it does not meet the requirements before proceeding with the identification of a new regression model with which to replace the one in use, it is good to analyse the data and check for the presence of outliers. The detection of the outliers is extremely important to create a model that is robust. The outliers are the data that have abnormal value, that are clearly distant from the majority of population example in figure 5.1, 3 or 4 times the standard deviation from the mean. The presence of these values could be linked to the measurement error or to the experimentation error, so it is good practice to check raw data before modelling. Sometimes due to the bad prediction performed by the model, some values could be classified as outliers and their elimination from the data set could bring to lose information on the process under investigation. Below are reported the method to avoid this, that were used during model creation by means of MBC and ASCMO.

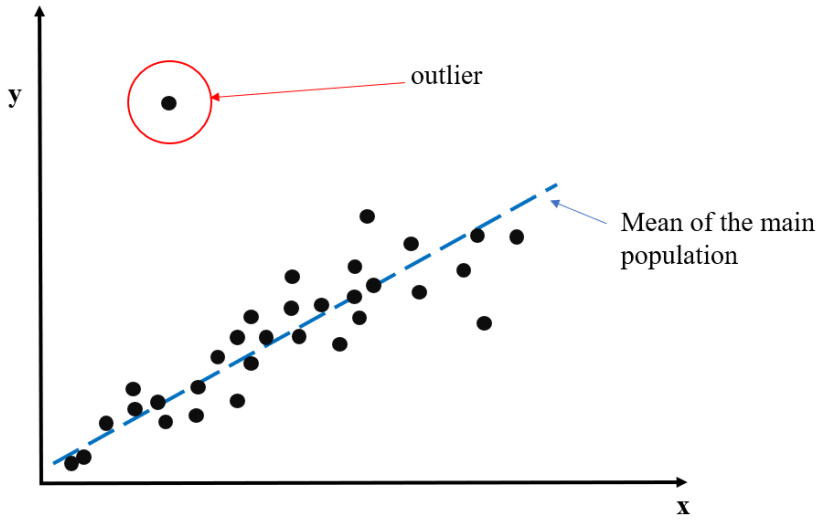

Figure 5.1- Example of outlier.

The simplest dis to verify graphically the presence of outliers by using the normal probability plot distribution. if the points in question are very different from the distribution, they may be outliers or it may be that the hypothesis that the data are normally distributed is wrong, therefore the elimination of the data would involve the loss of information. To prevent this from happening is important to check the studentized residuals versus

predicted response plot. In general, based on what suggest MBC guide, prediction that shows value of r_i greater than 3 can be considered as an outlier while in ASCMO the algorithm to detect the outliers is based on the value of the Standard deviation. Unfortunately, the elimination of the value under analysis is not automatic but must be done on the base of further considerations such as checking its plausibility and influence. One method to check the influence of data is the computation of the Cook's distance measure D_i whose expression is:

$$D_i = \frac{r_i^2}{p}\frac{h_{ii}}{(1-h_{ii})} \tag{5.22}$$

If the value of D_i is >1 the i-th observation must not be eliminated [13, p.339]. The value of D_i can be verified only on MBC while r_i is available for both the software.

5.5 Transformation

Transformation is a procedure that manipulate the variables of regression to adjust the non-normality and non-constant error variance that could lead in model that has standard error larger than necessary. "The effect of the transformation is usually to give more precise estimates of the model parameters and increased sensitivity for the statistical tests" [12, p.173]. The application of the transform re-expresses the relation between the regressor variable x and response. An important class of transformation of the response variable y is the power transformation: $y^{\lambda} = y'$ (y' transformed y) where λ is a parameter that must be determined. To determine the λ is possible to follow the method of Box and Cox [1964]. The procedure consists in apply the method of maximum likelihood in computing λ, this is equivalent in minimize the SSE. The practical computation of the λ value is:

$$y(\lambda) = \begin{cases} \frac{y^{\lambda}-1}{\lambda \dot{y}^{\lambda-1}}, & if\ \lambda \neq 0 \\ \dot{y}\ln(y), & if\ \lambda = 0 \end{cases} \tag{5.23}$$

Where $\dot{y} = ln^{-1}\left[\frac{\sum \ln(y)}{n}\right]$ that is the geometric mean of the observations. The transformation is present in both the software in particular the possible range λ in MBC is between -3 and 3 and in ASCMO from 1 to -1. In table 3.1 will be showed the equivalent transformed response variable for the most common choice of λ.

Value of λ	Transformed y
-3	$y^{-3} = 1/y^3$
-2	$y^{-2} = 1/y^2$
-1	$y^{-1} = 1/y$
-0.5	$y^{-0.5} = 1/\sqrt{y}$
0	log(y)
0.5	$y = \sqrt{y}$
1	y (no transform)
2	y^2
3	y^3

Table 5.1 - Typical value of scaling factor λ.

The value of λ must be chose in order to obtain the minimum of the SSE. In MBC is presents the possibility to verify if the SSE is minimized by means of SSE vs λ plot.

6. Experimental set-up

The experimental activity was performed in the ICE advanced laboratory of the Politecnico di Torino, in which a dynamic testbed is installed. In this chapter the characteristic of the analysed engine and description of the sensors, actuators and of the emission analyser will be done. The interface used to manage the actuators is possible through 4 computer stations equipped with software suitable for this purpose. Their utilization is summarised hereafter in the table number 6.1

ETAS INCA	Is the software that guarantees the interface with ECU. It allows to manage the calibration and to validate it.
AVL IndiCom	Adopted to monitor the combustion process and check its proper development by collecting the information directly from sensors.
AVL PUMA	Through PUMA are controlled the operations of the test bed such as the load applied by the dynamometer to the engine.
AVL CAMEO	Is the software designed for the automatization of the DoE launch procedure by communicating directly with PUMA

Table 6.1 - Description of the software compartment used in test procedure.

6.1 Engine

The engine used to perform the test is an F1A provided by FPT industrial. The engine is a light duty vehicle 2.4 litres 4 cylinder in line CI engine, equipped with a variable geometry turbocharger VGT with an exhaust flap downstream the turbine. The aftertreatment system ATS composed by cooled high pressure (HP) and low pressure (LP) exhaust gas recirculation EGR, diesel particulate filter DPF and oxidation catalyst DOC upstream of the selective catalyst reduction SCR. The SCR o is not used during the test phase. The engine has base calibration according to EURO 6 legislation limits.

Parameter	Value
Bore	88 [mm]
Stroke	94 [mm]
Max power	127 [Kw]
Max torque	400 [Nm]
Engine speed at max power	1500 [rpm]
Engine speed at max torque	3600 [rpm]

Table 6.2 - Technical characteristics of the engine.

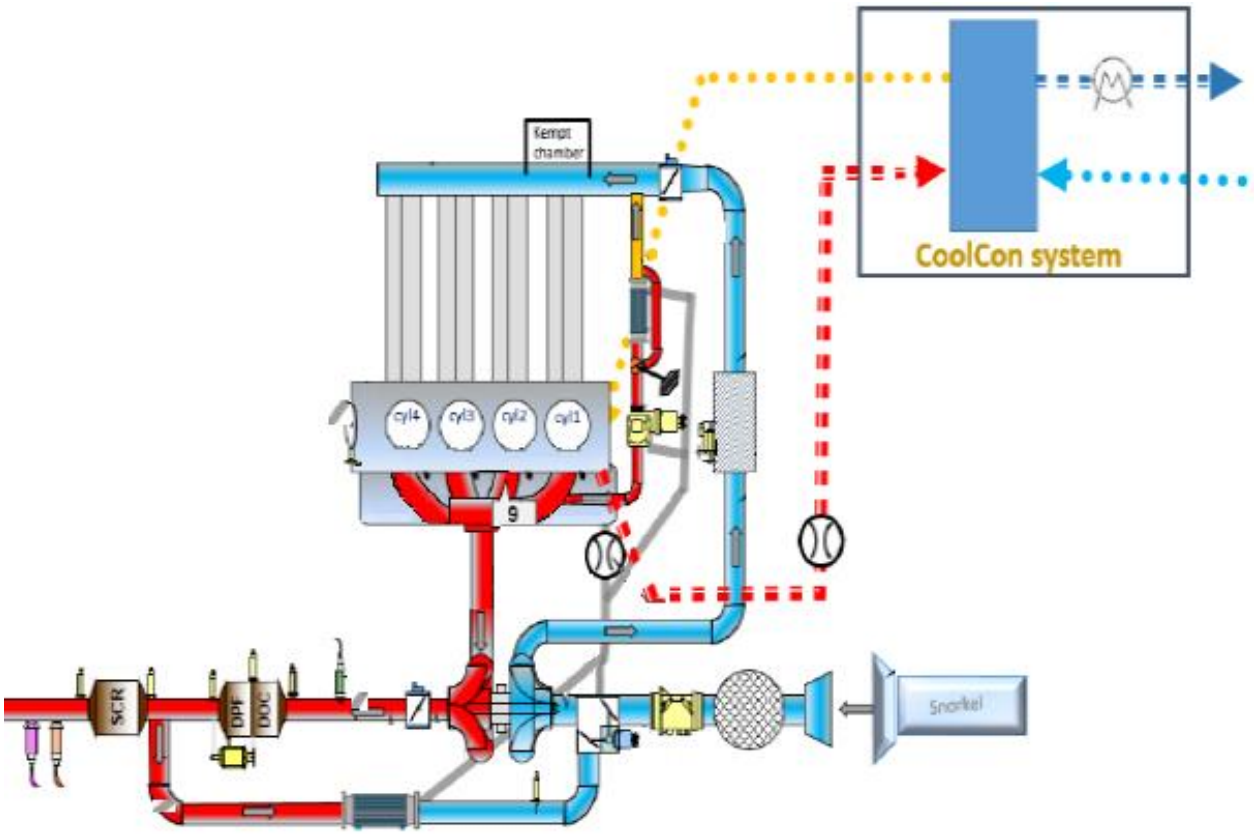

Figure 6.1- Engine layout and cooling system.

6.2 Dynamometer

The testbed is equipped with the dynamometer AVL APA 100. The dynamometer is capable to operate both as electric motor and as brake. In brake it applies a counter torque to the engine to simulate static and dynamic operative condition. In electric motor mode it is used to drag the engine in order to study its motored condition so to quantify the losses due friction.

Figure 6.2 - AVL APA 100 [17].

6.3 Engine cooling system

During the tests the engine is not coupled with a radiator, the cooling system is substituted by an external system integrated in the test cell. This system is called CoolCon, depicted in figure 6.1, has to replicate the function of the standard radiator in order to not affect the outcome of the test, since the temperature of the coolant influence the combustion process influencing the fuel consumption and the pollutant emissions. The CoolCon is composed by an- liquid heater that is used to heat the water that must be sent to cool the engine this procedure is done to speed up the warm-up phase of the engine before the start of the test. Is presents also a liquid-liquid heat exchanger that performs as the conventional role of the radiator. The system includes the delivery pump up which has the manual setting of the head upstream of the engine one and a water recirculation pump to compensate the losses in the circuit. The flow rate of the coolant fluid in the liquid-liquid heat exchanger is managed by a proportional-integral-derivative PID controller. The PID stabilize the temperature of the coolant to the one selected by the operator usually 85 °C.

6.4 Fuel metering system

The measurement of the fuel flow directed to the engine, is an important information that allows the computation of the fuel consumption. The metering system is the AVL KMA 4000. The system is composed by the PLU measuring unit, filter, heat exchanger inlet and outlet pump and density sensor. The fuel is sent by an external pump to the KMA 4000 the pump embedded sends fuel to the fuel metering unit and the outlet one then delivers fuel to the engine rail system. The fuel from the rail is sent to the heat exchanger and then back to the tank. The mass flow rate of the fuel is computed using the data acquired by the metring unit and by the density sensor.

6.5 Sensors

alongside the normal sensors already present in the engine and controlled by the electronic control unit ECU, further sensors mainly for temperature and pressure have been added. the calibrations of these additional were uploaded to PUMA. Hereafter in this section the sensors used for the acquisition of data are described.

6.5.1 Pressure sensors

In the engine were mounted different pressure sensors the ones that are in the most critical positions will be described. These positions are: combustion chambers, intake manifold and exhaust manifold. The sensors located in those areas are subjected to high frequency pressure variation and high temperature reached. The one mounted in the combustion chamber is the Kistler 6058A this sensor is a piezo-resistive and needs electronic amplifier to allows the filtering of the noise. The one mounted in the intake manifold is the Kistler 4007C this piezo-resistive sensor working principle is based on a Wheatstone bridge to generate an electrical signal proportional to the pressure [13]. The Kistler 4049B is mounted in the exhaust manifold is a self-cooled sensor. Below in the table are described the main features of the sensors.

Model	Pressure range [bar]	Temperature range (min/max) [°C]	Cooling fluid flow [l/min]
Kistler 6058A	0 ÷250	-50 / 400	-
Kistler 4007C	0 ÷ 250	0 / 250	-
Kistler 4049B	0 ÷ 10	0 /120	0.3÷0.5

Table 6.3 - Pressure sensors technical data [18].

6.5.2 Temperature sensors

The temperatures sensors adopted are of two kind thermistor and thermocouple. The first are based on the principle of the variation of their electric resistance related to temperature changes, so the voltage drop across them varies consequently. The type adopted in our case were the PT100 with a resistance of 100 ohm at 0°C. The thermocouples which in our study were used for measuring the fluids temperatures, instead works on the base of the Seebeck effect for converting heat in electricity. Practically a voltage difference takes place when 2 different conductors are in contact and subjected to a temperature gradient, this voltage since is small is amplified and measured. The usage range of the thermocouples varies from -270 to 1370 °C.

6.6 Emissions measurement systems

Since the one main goal of this work is to find an optimization in terms of main pollutant emissions and fuel consumption for specific engine working points, in this section will be discussed the working principle of the main instrument used to measure the pollutant emissions. The collected gaseous emissions are collected in raw form, so without air dilution, to prevent the acquisition of misleading results the reaction of the collected pollutant must be avoided. Moreover, the presence of water vapour must be avoided since the measurement instrument are of the dry type and solid particulate are eliminated through. The device used for the emissions measurement is the AVL AMA i60. The apparatus is endowed with three heated sapling lines that take the gaseous emissions in three different points. The first line extract before the ATS the second after the ATS while the third one samples at the intake to measure the CO_2 concentration to calculate the EGR percentage. For what concern the soot emission the measurement is carried out with the smoke meter AVL 415S.

6.6.1 CO and CO_2 measurement

To perform the analysis of the CO and CO_2 the Non-Dispersive Infrared Detector NDIR are used. The working principle of this devices is based on the gases absorption capabilities of a radiation of specific wavelength in the infrared region. Besides the gas that has to be analysed a reference gas is needed, it is an inert one usually nitrogen that has low absorbing properties. The system is composed by two volumes. One volume made of two independent chambers one containing the inert gas called reference cell and the other the sample gas called sample cell. The second volume made of a third chamber called the detecting cell. Both the independent chambers are exposed to the radiation source and absorb part of the radiation that reach the detecting cell, that is divided in two halves by a membrane that is undeformed because the pressure in both is equal. Each half faces only one of the previous cells. This third chamber is filled with the same gas to be analysed in both the halves. Since the past infrared radiation has yielded part of its energy in different quantities, to the two gases previously exposed to it, the gas contained in the halves of the detecting cell will be heated accordingly.

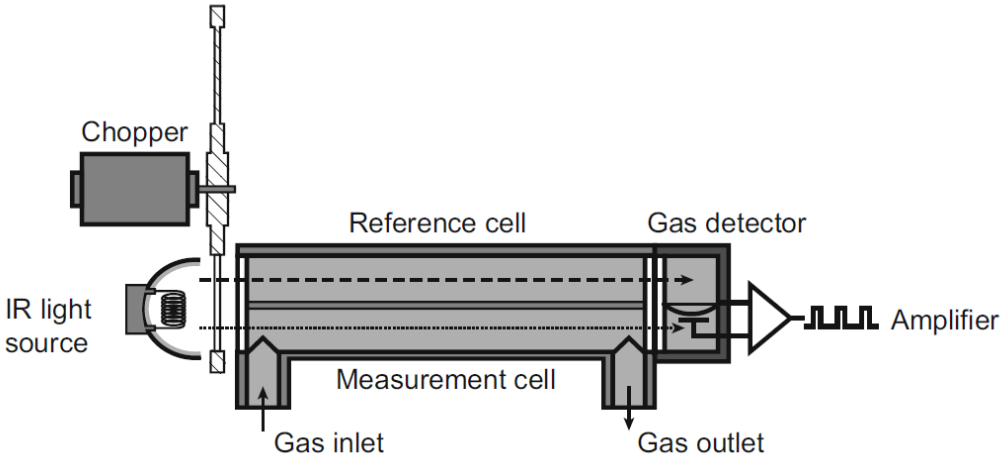

Figure 6.3 - NDIR scheme [19].

The different heat absorbed by the two halves imply a pressure difference that deforms the membrane. The deformation is converted in an electrical signal proportional to the sample gas concentration. In order to obtain a signal that is easy to elaborate the radiation is modulated by means of a rotating chopper interposed between the two volumes, in this way the membrane start to oscillates generating an alternate current.

6.6.2 NO and NOx measurement

The NOx measurement is based on the principle of the chemiluminescence for which a molecule that passes from an exited electronic state to a lower ground by emitting heat and light. In particular reaction of NO with the O_3 ozone that is obtained is obtained by sampling ambient air that pass through an ozone generator. The products of these two reagents are the NO_2^* in excited state plus O_2, subsequently the NO_2^* stabilizes and returns to NO_2 by doing so photons are emitted [15]. This reaction happens in the reaction chamber of the chemiluminescence detector CLD and the light emitted is measured and amplified by a photomultiplier so the electrical signal is proportional to the NO concentration. To measure the NOx concentration the sample gasses before entering the reaction chamber pass through the NOx converter in order to have all the NOx reduced to NO. The measurement of NOx and NO can be done by using a system composed of two different reaction chambers one in which the sample gas has passed through the NOx reducer and the other in which the sample gas is injected directly. In both the typology the NO_2 measure can be derived by subtraction between the two concentrations.

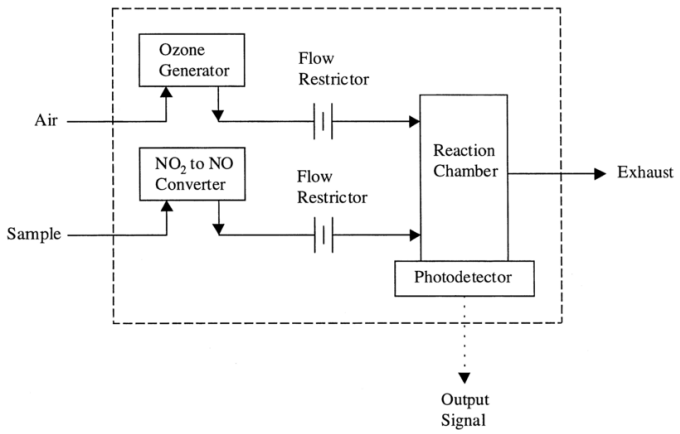

Figure 6.4 - chemiluminescence detector CLD schematic diagram [20].

6.6.3 HC measurement

The quantification of the emissions of unburned hydrocarbon HC is entrusted to Flame Ionization Detector FID. The FID is based on the awareness that the combustion of hydrocarbons releases a relevant number of ions that are proportional to the carbon atoms. the FID is composed by a burner in which hydrogen is combusted, the flame products are directed toward collector electrodes. Since the hydrogen combustion do not produce ions the electrodes remain at equal potential with no current flowing between them. During the measurement also, the sample gas flow in the FID. During this phase the ions released are totally related to the combustion of the HC, these released ions generate an electric differential potential that generates a flow of current in the electrodes proportional to the HC concentration

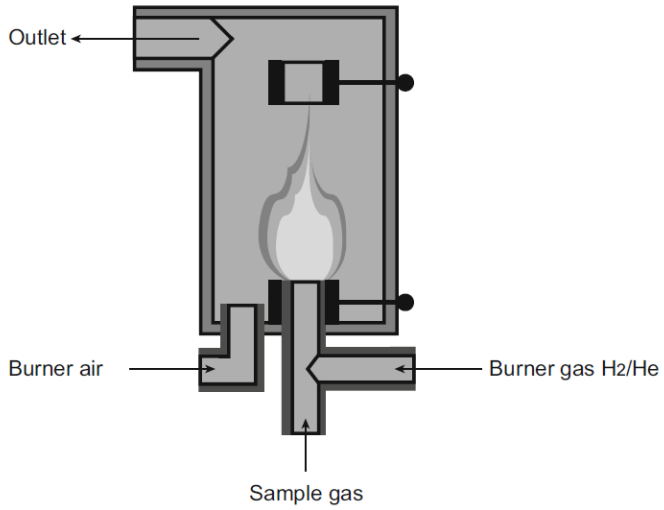

Figure 6.5 - FID layout [19].

6.6.4 O_2 measurement

The O_2 estimation is important to establish the correct quantity of fuel to be injected to have the target air fuel ratio and to quantify in a precise way the amount of EGR. Alongside the engine's lambda sensor that is used to analyse the quantity of oxygen in the exhaust gases but more precise estimation of the air fuel mixing can be done from the exhaust gas analysis. The Lambda sensor is mounted downstream the turbine outlet before the ATS. Its measurements provide a reliable indication of the lambda (air fuel ratio) that is used to estimate the quantity of fuel to be injected each cycle used by the engine. The lambda sensor used in our case is the universal exhaust gas oxygen UEGO. The analysis of the exhaust gas by means of the Paramagnetic Oxygen Detector POD uses the paramagnetic property of the oxygen. The device is composed by chamber containing two diamagnetic quartz spheres containing nitrogen connected each other by an arm. The two spheres are within a string magnetic field and are mounted on a rotating axis. On the axis a mirror is mounted that reflect the light coming from a light source toward light sensor. When the sample gas is allowed to flow into the chamber the oxygen present in the gas flows toward the magnetic field displacing the spheres and causing the arm rotation. The rotation is detected by the light sensor. The system is maintained in central position by a control unit. The current required by the control unit to apply a sufficient counter torque is proportional to the O_2 concentration.

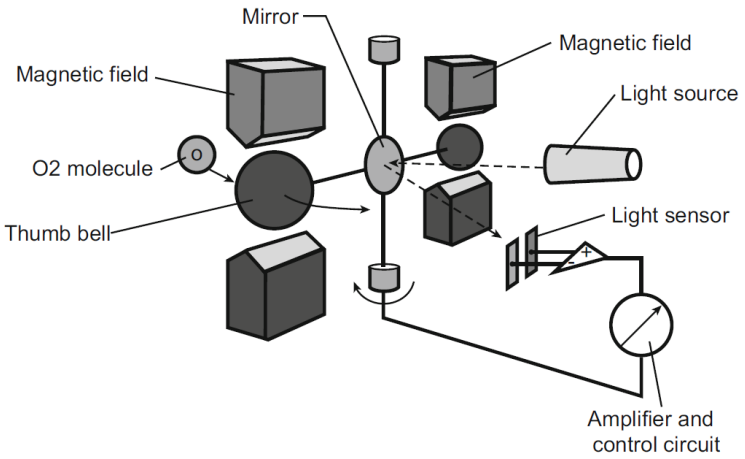

Figure 6.6 - POD layout [19].

6.6.5 PM measurement

For the PM measurement smoke meter is adopted. This instrument can be used only for measurements in the steady state condition therefore it turns out to be very suitable for the type of study carried out. In the smoke meter the exhaust sample gas passes through a white paper filter. Light coming from a photodiode is impressed on the dirty filter and the resultant reflected by the filter is measured by a receiver. The amount of reflected light depends on the blackening of the filter due to the filtered soot This procedure gives the filter smoke number FSN [21].

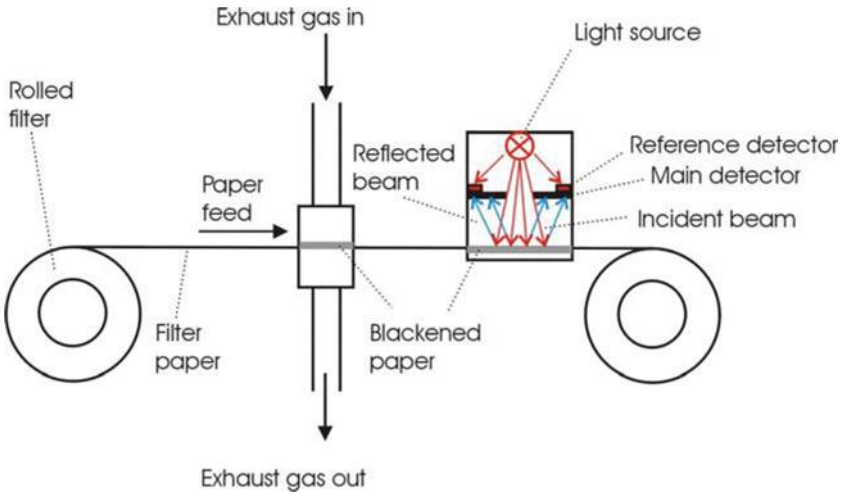

Figure 6.7 - Smoke meter scheme [22].

7. Modelling

This chapter contains the description of the tested engine working points, starting from the selection of constraints, defined considering the results of the preliminary tests. Then the method followed for the creation of the variation list and regression models used in MATLAB tool MBC and ASCMO will be discussed. Lastly a comparison will be made between the optimizations obtained with the two software for both types of fuel, verifying that outputs obtained are close to the experimental ones. In figure 7.1 the overall strategy followed during the development of this work is reported.

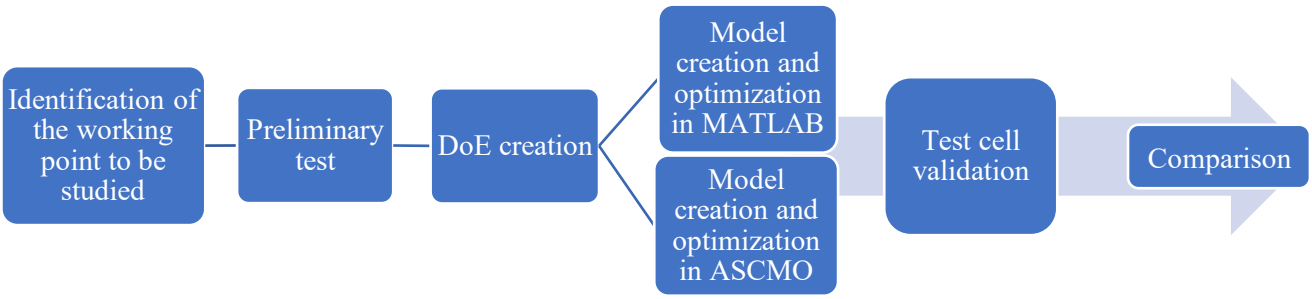

Figure 7.1- Procedure workflow

The operating point that will be discussed are:

- 1250[rpm] x 36 [Nm]
- 2000[rpm] x 163 [Nm]
- 2250[rpm] x 274 [Nm]

Each of them was tested using both HVO and standard diesel fuel B7 EN590. These operating points can be considered ad representative of different operating ranges of the engine. They are respectively low load for 1250x36 point with 13% of the maximum torque available at the current regime, average load for 200x163 with 46% of the maximum torque and high load for 2250x274 with 78,3%.

7.1 Preliminary tests

The step that anticipates all the work of creating the local model is to perform the preliminary tests for each point. This procedure was performed twice for all the operating points since two types of fuels were used. The tests are needed to study if the combustion is affected by the variation in a certain range of some parameters, in terms of stability of combustion. This allowed us to restrict the domain of the space design on which the DoE was created. The preliminary test helped us to confirm the choice of the most influential parameters, that had been selected based on the experience of the research team on an engine with similar characteristics and layout. Since the EGR rate can have influence on the NO_x-soot trade off, the combined actuation of the two layout HP EGR and LP EGR must be verified, especially if they are matched with a VGT [23]. Therefore, particular attention was paid to the constraints of the HP EGR and LP EGR valves actuation. The inputs and their variation range are reported in tables 6.1.

Fuel	Input	Working point			Unit
Diesel		**1250x36**	**2000x163**	**2250x274**	
	SOI main	-5 ÷ -1	-4.4÷ -0.4	1.5 ÷ 3	[deg bTDC]
	qPil1 (quantity of pilot 1)	1 ÷ 3	1 ÷ 3	0.4 ÷ 3	[mg/str]
	tPil1 (dwell time of pilot 1)	890 ÷ 1290	867 ÷ 1000	450 ÷ 1000	[µs]
	Rail pressure set point	410 ÷ 810	1100 ÷ 1600	1200 ÷ 1700	[bar]
	VGT	87 ÷ 96	65 ÷ 90	55 ÷ 75	[%]
HVO					
	SOI main	-5÷ -1	-4.4÷ -0.4	1.5 ÷ 3	[deg bTDC]
	qPil1 (quantity of pilot 1)	1 ÷ 3	1 ÷ 3	0.4 ÷ 3	[mg/str]
	tPil1 (dwell time of pilot 1)	890 ÷ 1290	867 ÷ 1000	450 ÷ 1000	[µs]
	Rail pressure set point	410 ÷ 810	1100 ÷ 1600	1200 ÷ 1700	[bar]
	VGT	87 ÷ 96	65 ÷ 90	55 ÷ 75	[%]

Table 7.1 - Working points inputs variation range

The HP and LP constraints for each working point are shown in the figures 7.2 ,7.3 and 7.4 both for HVO and diesel. It can be seen that the constraints used for the two fuels limit the operative area of the two EGR systems in similar way, with small differences that are negligible. Those area were obtained by testing several combinations of the two EGR loops actuations valves and seeing how the lambda value drifts from the optimal values selected according to the engine base calibration map for each of the operating points. These limits will then be entered in MBC to establish the range in which the inputs must vary to create the DoE.

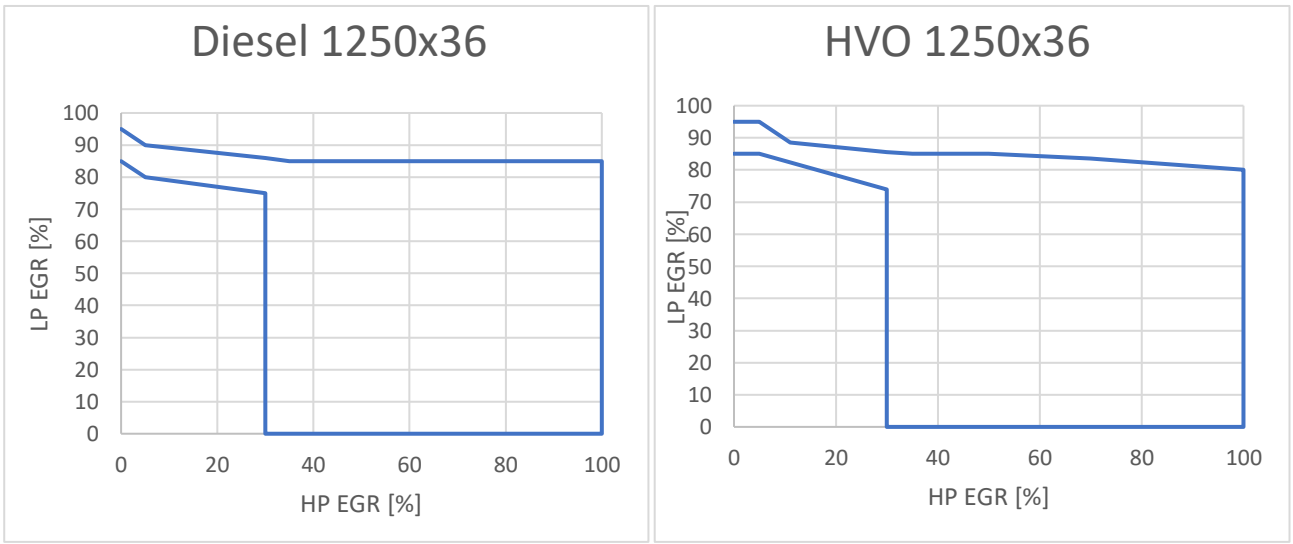

Figure 7.2 - 1250x36 LP EGR and HP EGR valve actuation constraints.

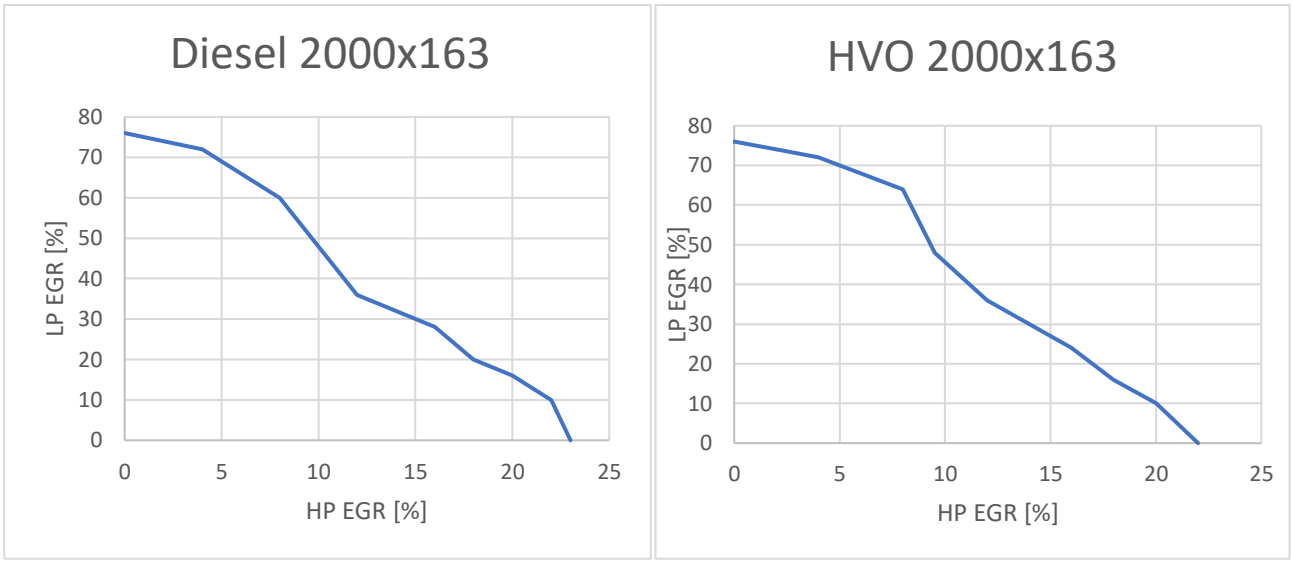

Figure 7.3 - 2000x163 LP EGR and HP EGR valve actuation constraints.

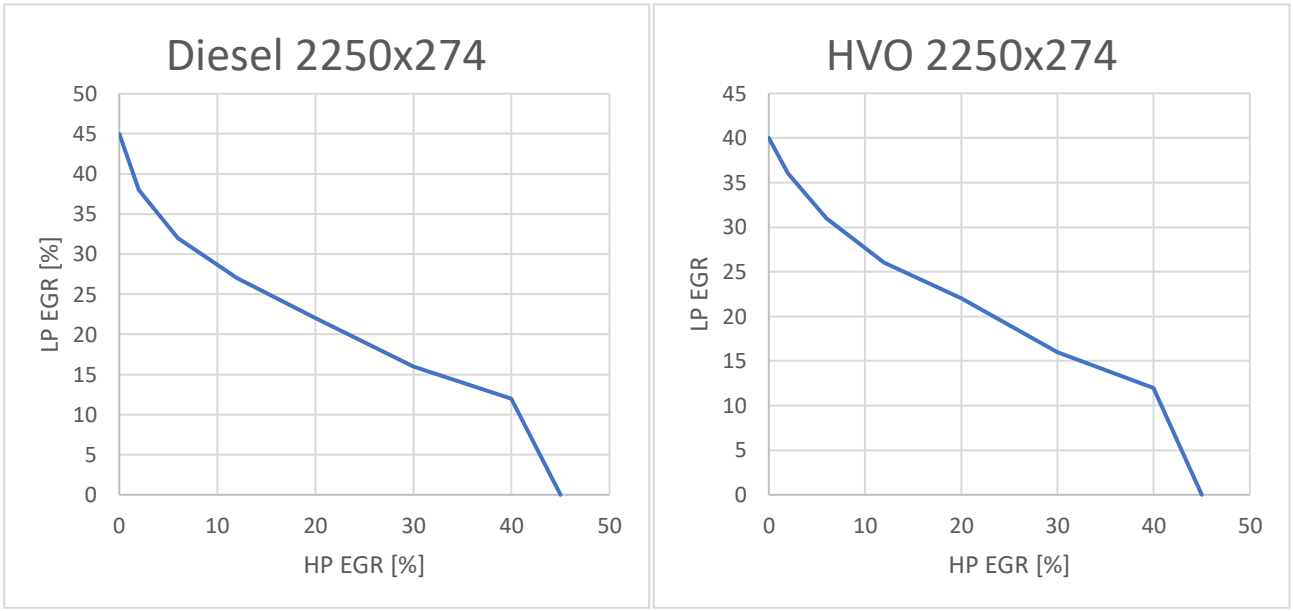

Figure 7.4 - 2250x274 LP EGR and HP EGR valve actuation constraints.

7.2 DoE creation

Among the various methods available to build the variation lists, the choice fell on the V-optimal method. The optimal design methods as described in previous chapter are the more suitable to create the variation list in presence of constraints in the space design of the inputs. Also, is worth to add that the optimal design was used by the research team in previous works, therefore it represents the best known and tested method. The first step regards the selection of the regression model to be used. Starting by imposing the 7 inputs chosen and their relative range of variation, the next step regards the selection of the polynomial order, which we imposed to be of the second order. In general, a good approach in creating the regression model is to enable the stepwise function adopting as method for the minimization of the PRESS as depicted in figure 7.5. The stepwise function consists in selecting the most useful input variables to be included in the regression model during the fitting,

so this choice goes beyond the creation of the Doe variation list but it will be useful during the model fitting procedure

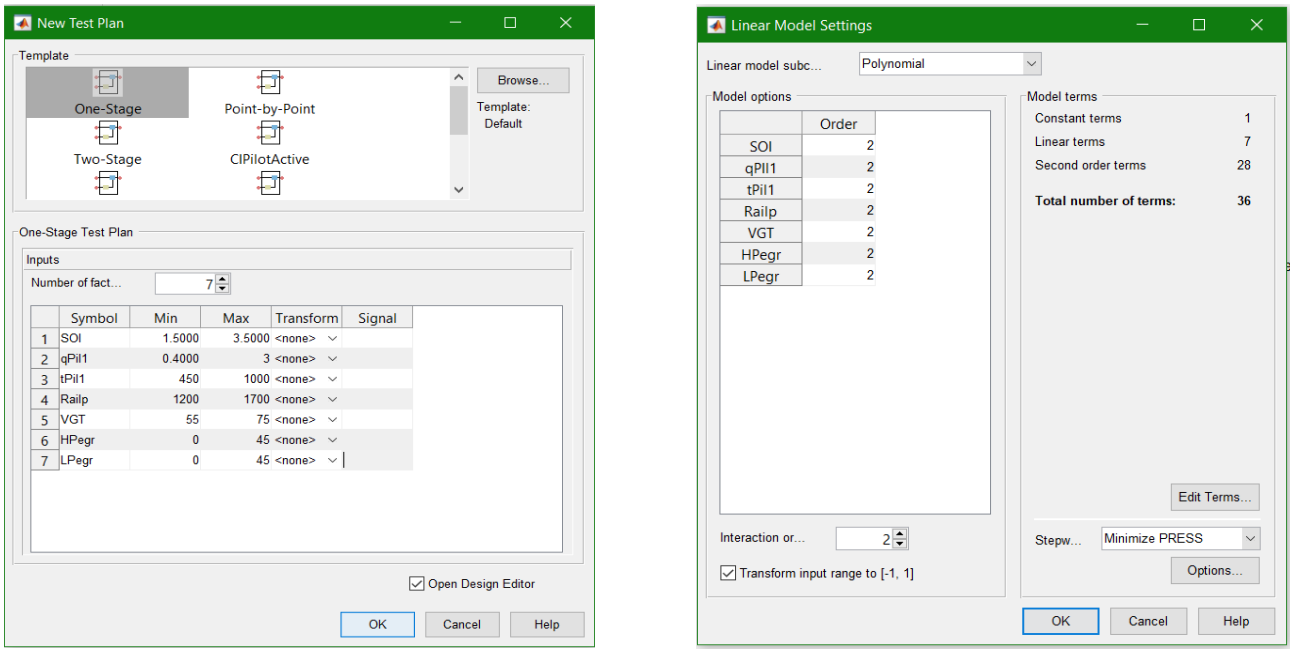

Figure 7.5 - Selection of the number of input of the DoE on left and regression model selection on right side.

Therefore, after having imposed in advance the use of a linear polynomial predictive model, it is possible to set the parameters of the V optimal design. The number of testing points of the variation list, thanks to the V optimal method was reduced down to 130. This number of tests considering 7 input variables was the one that ensure good minimization of the PEV (predicted error variance), whose value is reasonably to be maintained below 1 for all the design domain especially in the edges where usually the highest value is reached, we tried to keep it minor 0.2 on average.

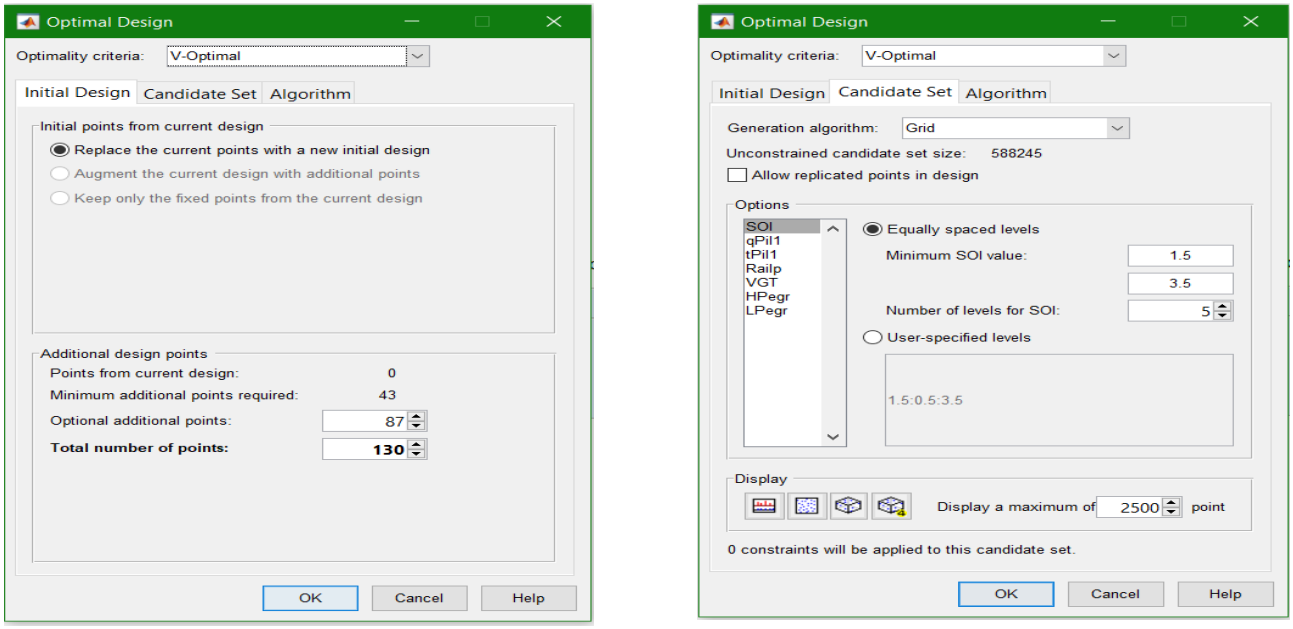

Figure 7.6 - Selection of the optimal criteria DoE number of points on the left, selection of input levels on the right.

For each of the input variables it is important to select the number of levels that each of them must have (figure 7.6). The selection of the levels is important, since a too thick division into levels could causes the number of tests to increases to have an effect on the variation of the output that would be visible, while a too large division into levels would omit siganficative combinations. This choice is mainly linked to the choice of those who carry out the study based on their own preavious experience. Furthermore, the trust limit of the system must be taken into account, therefore the limit linked to the accuracy of the actuators. For example in the specific case of point 2250x374 it seemed reasonable to divide the SOI variation into 1 degree steps, while the rail pressure was made to vary in step of 100 [bar], as smaller variations are not reacheble by the installed common rail system. Last step of the DoE construnction is the definiton of the input constrains as shown in particular in figure 7.7.

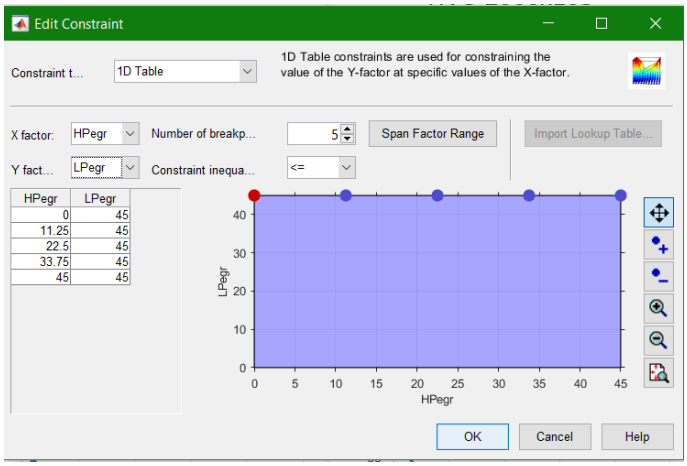

Figure 7.7 - Definition of the constraint on HP EGR and LP EGR.

After having found the required 130 points they were randomized so that during the tests there were no influences due to external disturbing factors. 10 more points are added later in the variation list by hand. These points are very important to see if there is a drift in the results due to external factors such as the need of DPF regeneration. In order to have this analysis, all these 10 points have equal value. For this reason, it was decided to consider as a repetition point the one of the base calibration in the operating point under study. When the variation list is completed the tests are launched and the results are collected and then elaborated to be inserted in MBC.

7.3 MBC procedure for model fitting

The test results are collected and inserted in MBC figure 7.8. The affected outputs are assigned to the variables and the predictive model is created for each of the following outputs:

- CO brake specific carbon monoxide emissions [g/kWh]
- NOx brake specific nitrogen oxides emissions [g/kWh]
- CN combustion noise [g/kWh]
- Soot brake specific soot emissions [g/kWh]
- Lambda relative air fuel ratio
- bsfc brake specific fuel consumption [g/kWh]
- HC brake specific unburned hydrocarbon emissions [g/kWh]

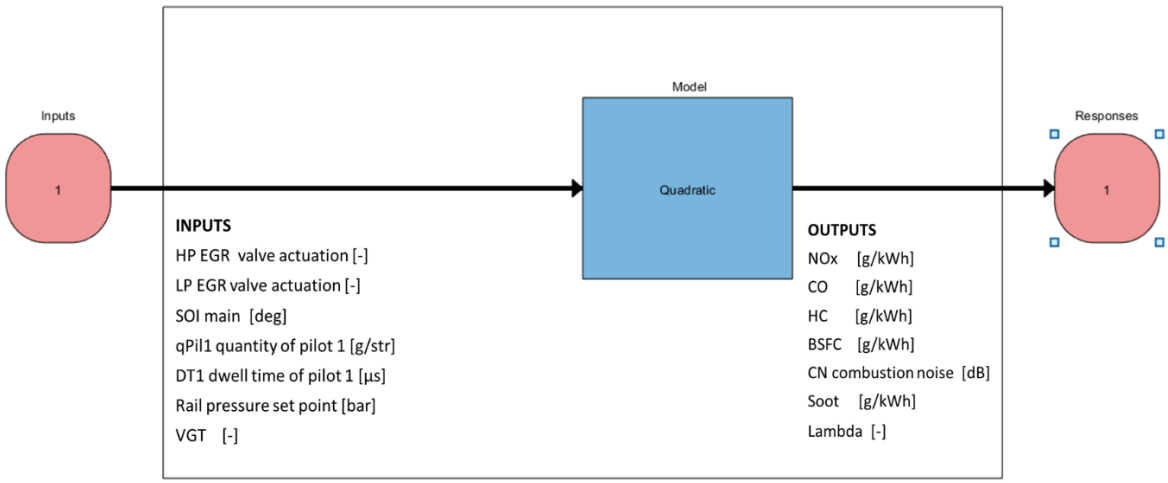

Figure 7.8 – Model test plan.

Of the studied points we are interested in knowing if they meet certain criteria that evaluate their predictive capacity of the real system, these criteria are the main statistical indicators afore mentioned in chapter 5. The principal is the coefficient of determination R^2 of which we have taken as optimal a minimum value to be reached, that is 0.80 for all the responses. The R^2 is also a parameter that allow us to us to evaluate one model over another and choose the best among them. If a model does not satisfy this criterion, it would be retrained after that the operations described in the workflow of the figure 7.9 have been carried out.

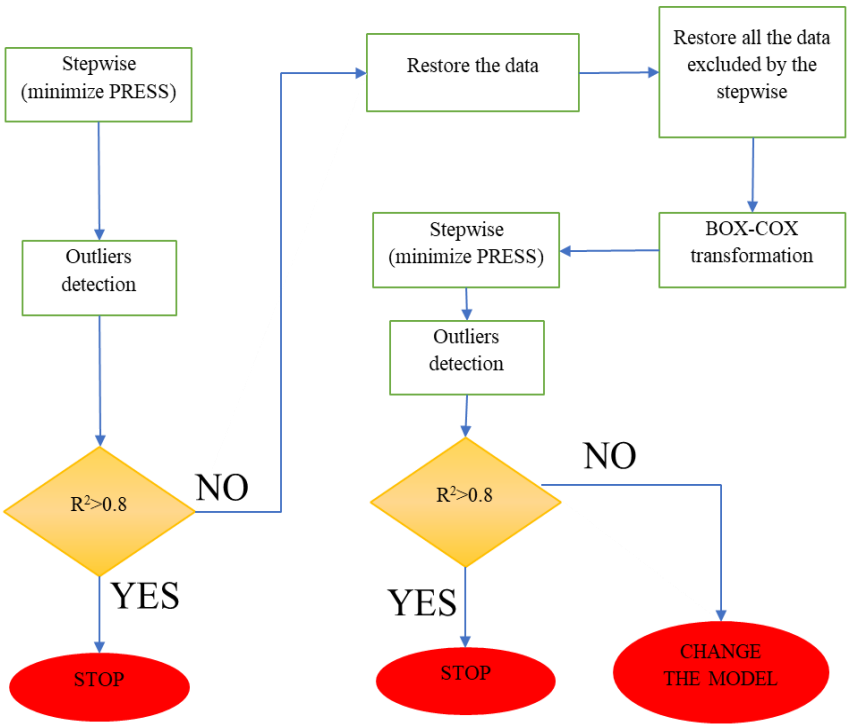

Figure 7.9– Procedure of model improvement [24].

Another operation done in parallel is the check of PEV surface by means of the PEV view in MBC figure 7.10.

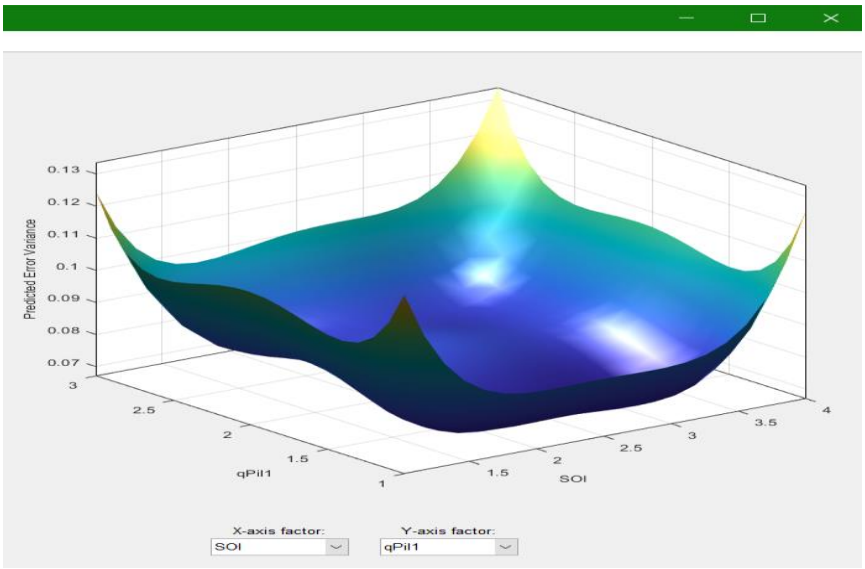

Figure 7.10 – PEV surface view.

This give us straight information of the maximum value of the PEV obtained called G and its average called V. Referring to the figure 7.9 a basic operation to always carry out is the control of the outliers. In our case the criterion adopted to identify values as outliers which proved to be satisfactory was already used by the research team. This criterion consists in satisfying 3 conditions at the same time:

- $|r_i| > 3$
- $D_i < 1$
- $D_i < 0{,}5 * D_{MAX}$ where D_{MAX} is the maximum Cook's distance

The data identified as outliers are eliminated from the model training. Even if some data are considered outliers on the base the above criterion it is not convenient to delete them if the value of R^2 is already satisfying since it could cause overfitting. Statistical indicators can direct one into a wrong choice if their values are observed without contextualizing them. For example, a high value of R^2 not always indicate that the model has good predictive capabilities but may indicate that the model is well fitted for that specific data set with whom the model has been trained on so it is affected by overfitting. Therefore, it is a good idea to check the versatility of the model by giving a new set of data, called test data set, to test the model predictive capability. This test data must be independent from the one used for training the model. These data are compared with the model obtained with training data and by evaluating the resulting RMSE it is possible to quantify how much the model suffers of overfitting. In our case if the RMSE value of the test set was maximum four times that of the training the model is considered good with some exceptions taking into account the nature and number of data tests given. The data set used as test was taken from the preliminary test data of each operating point. The points of preliminary tests have the disadvantage of having been taken at different stages since when the DoE for each operating point was launched, therefore they belong to populations of data obtained under different conditions. The choice that led us to using the preliminary tests was weighted on the basis that their use brought savings in terms of experimental time, as they were already available. In addition, the fact that they belong to another data set did not affect the number of data used for model training, because if a part of these had been used for the test they would not have been used for the creation of the model. The resulting statistical indicators and response of the model will be reported and discussed below.

7.3.1 1250x36

The point 1250x36 showed criticalities for what concern the bsfc and the HC models. For these two particular models the obtained R^2 was well below value of 0.80 but it was decided to maintain them as well since for both the option of adopting a more complex model or different Box-Cox transformation have resulted only in overfitting especially for HC table 7.2. The bad HC results can be attributed to low emission registered by the sensors that could not register the low variation of this pollutant.

Response model statisics 1250 [rpm] x 36 [Nm] diesel								
Name	**Unit**	**Box-Cox**	**PRESS RMSE**	**RMSE**	**R^2**	**R^2adjusted**	**PRESS R^2**	**Test RMSE**
Lambda	[-]	-1	0,168	0,133	0,903	0,871	0,785	0,160
CO	[g/kWh]	-1	0,616	0,487	0,865	0,822	0,731	0,940
Soot	[g/kWh]	-0,5	0,017	0,015	0,891	0,873	0,846	0,017
bsfc	[g/kWh]	1	2,492	2,185	0,781	0,710	0,620	2,965
CN	[dB]	1	0,519	0,432	0,926	0,902	0,858	0,369
NOx	[g/kWh]	1	0,359	0,327	0,903	0,890	0,866	0,471
HC	[g/kWh]	1,5	0,209	0,196	0,559	0,493	0,415	0,295

Table 7.2 – Statistical indicators polynomial model MBC 1250x36 diesel.

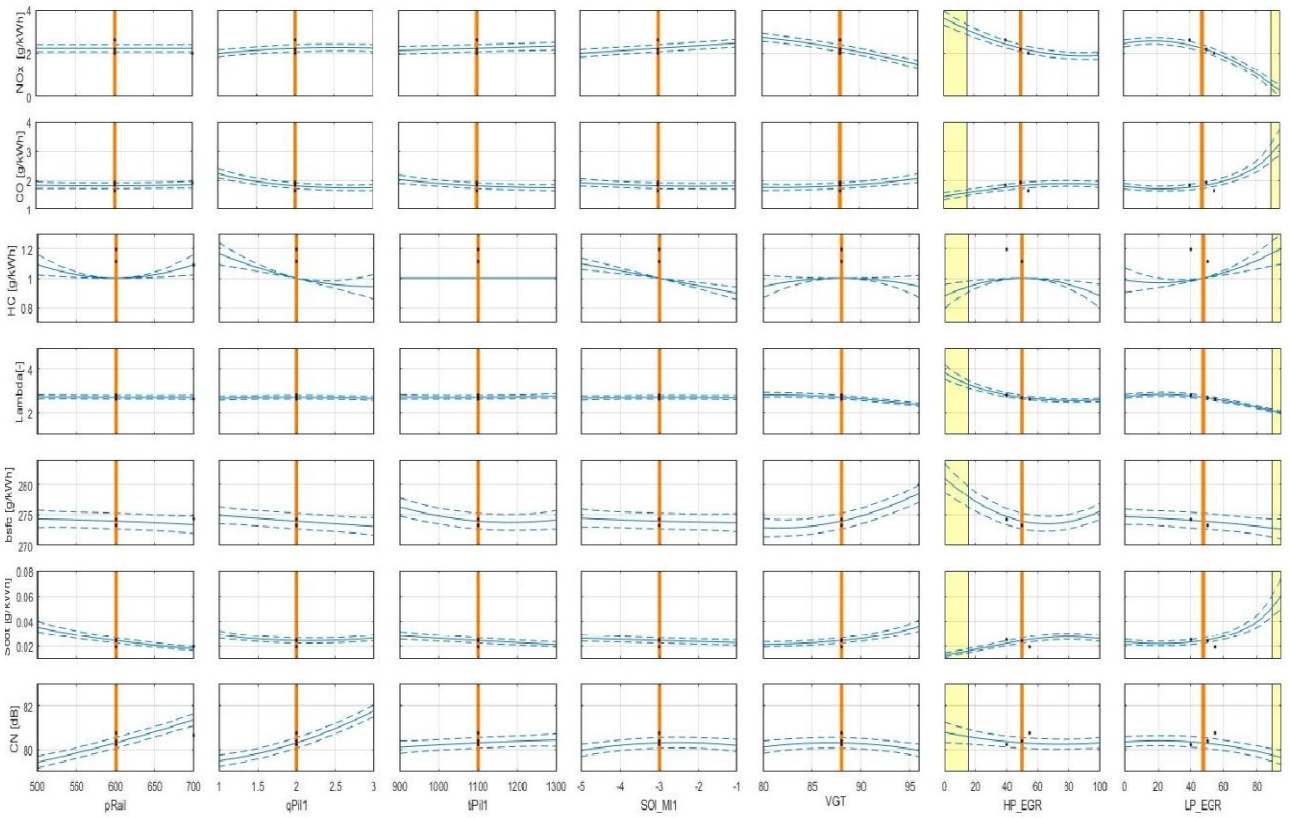

Figure 7.11 - Response polynomial model MBC 1250x36 diesel.

For the HVO models this inconvenience not occurred (table 7.3). One reason can be attributed to the fact that the tests carried out with HVO fuel were carried out at lower cell temperatures than those carried out with conventional diesel fuel. This handicap is due to the fact that the entire study was carried out in the absence of the air conditioning system of the cell due to the breakage of the latter. The differences between the two regressions quality can be seen looking at their response in figure 7.11 and 7.12. In particular we can observe that for the diesel (figure 7.11) the HC responses it cannot detect any influence of the input tPil1 (dwell time

of the pilot1) so it is represented as a perfect horizontal line without information on the confidence level (dashed line).

Response model statisics 1250 [rpm] x 36 [Nm] HVO								
Name	**Unit**	**Box-Cox**	**PRESS RMSE**	**RMSE**	**R^2**	**R^2adjusted**	**PRESS R^2**	**Test RMSE**
Lambda	[-]	1	0,156	0,126	0,893	0,860	0,783	0,164
CO	[g/kWh]	1	0,291	0,242	0,893	0,860	0,795	0,261
Soot	[g/kWh]	-0,5	0,012	0,009	0,936	0,916	0,873	0,008
bsfc	[g/kWh]	1	2,242	1,879	0,824	0,769	0,670	3,303
CN	[dB]	1	0,355	0,299	0,962	0,950	0,929	0,363
Nox	[g/kWh]	1	0,408	0,335	0,906	0,877	0,816	0,441
HC	[g/kWh]	1	0,051	0,043	0,820	0,764	0,671	0,039

Table 7.3 - Statistical indicators polynomial model MBC 1250x36 HVO.

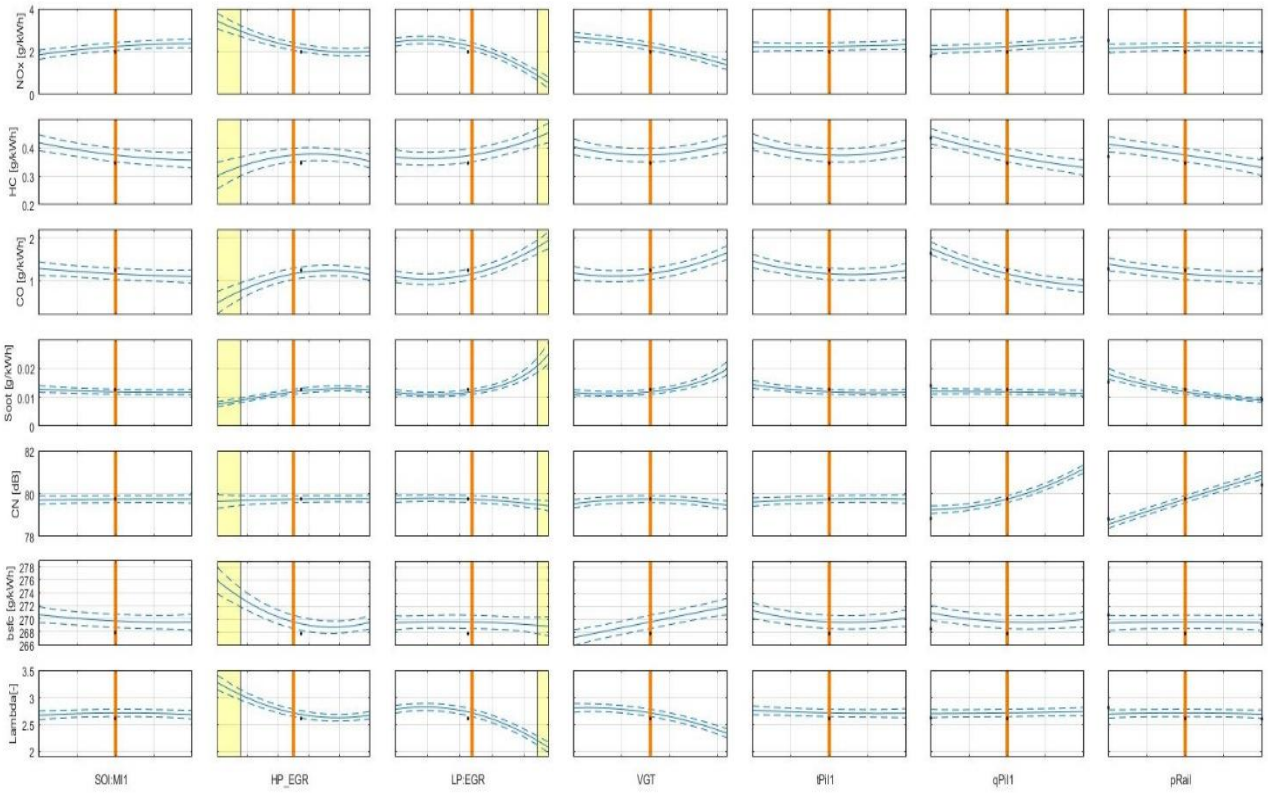

Figure 7.12 – Response polynomial model MBC 1250x36 HVO.

7.3.2 2000x163

The results of this point are characterized by good value of R^2 for all the responses but HC for the reasons above mentioned.

Response model statisics 2000 [rpm] x 163 [Nm] diesel								
Name	**Unit**	**Box-Cox**	**PRESS RMSE**	**RMSE**	**R^2**	**R^2adjusted**	**PRESS R^2**	**Test RMSE**
Lambda	[-]	1	0,051	0,043	0,983	0,977	0,968	0,073
CO	[g/kWh]	0	0,193	0,179	0,927	0,917	0,902	0,078
Soot	[g/kWh]	0	0,040	0,036	0,960	0,954	0,945	0,032
bsfc	[g/kWh]	1	1,066	0,893	0,984	0,979	0,969	2,015
CN	[dB]	1	0,277	0,234	0,992	0,989	0,984	0,256
NOx	[g/kWh]	1	0,372	0,317	0,981	0,975	0,965	0,197
HC	[g/kWh]	1	0,018	0,017	0,544	0,485	0,412	0,017

Table 7.4 - Statistical indicators polynomial model MBC 200x163 diesel.

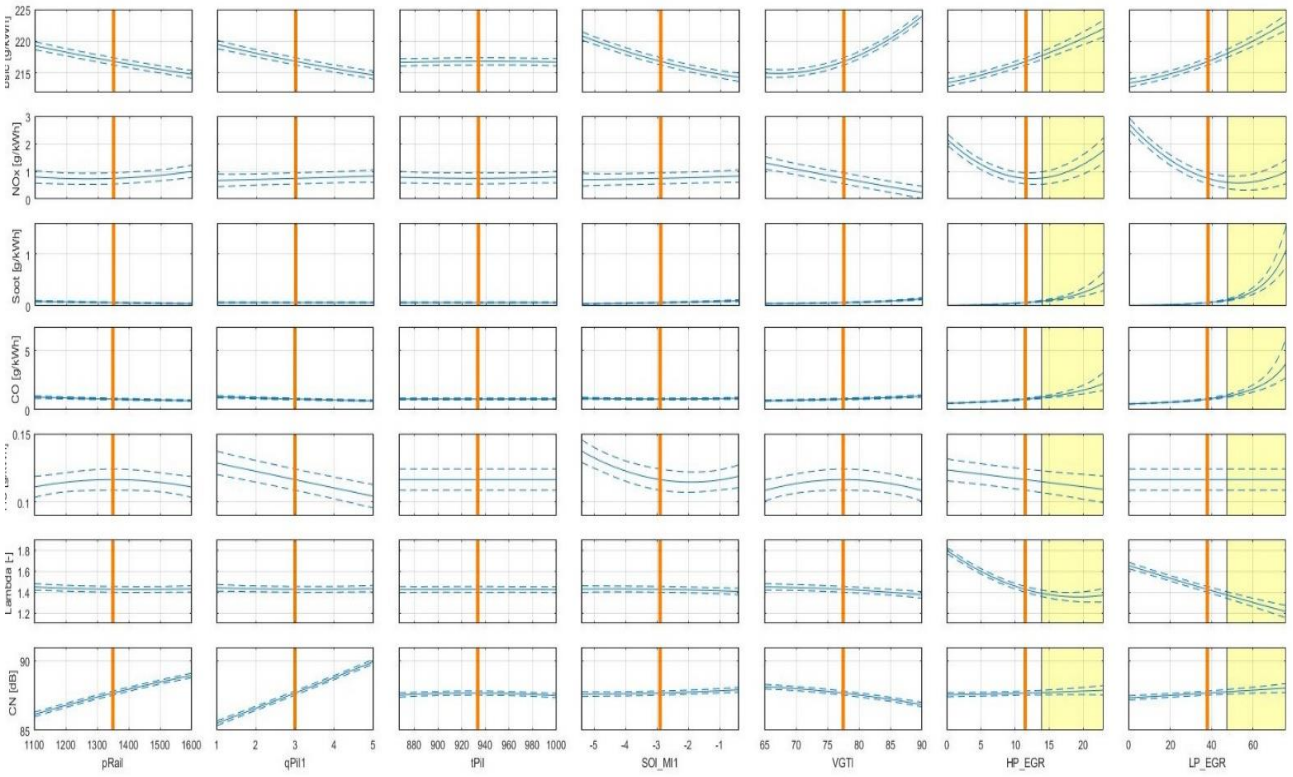

Figure 7.13 – Ressponse polynomial model MBC 2000x163 diesel.

Response model statisics 2000 [rpm] x 163 [Nm] HVO								
Name	**Unit**	**Box-Cox**	**PRESS RMSE**	**RMSE**	**R^2**	**R^2adjusted**	**PRESS R^2**	**Test RMSE**
Lambda	[-]	1	0,048	0,040	0,985	0,979	0,969	0,140
CO	[g/kWh]	-0,5	0,184	0,153	0,971	0,960	0,941	0,324
Soot	[g/kWh]	0	0,030	0,025	0,974	0,964	0,945	0,109
bsfc	[g/kWh]	1	1,033	0,868	0,988	0,983	0,976	1,930
CN	[dB]	1	0,273	0,222	0,990	0,987	0,980	0,126
NOx	[g/kWh]	1	0,368	0,302	0,981	0,973	0,960	1,169
HC	[g/kWh]	1	0,006	0,005	0,816	0,778	0,718	0,010

Table 7.5 - Statistical indicators polynomial model MBC 200x163 HVO

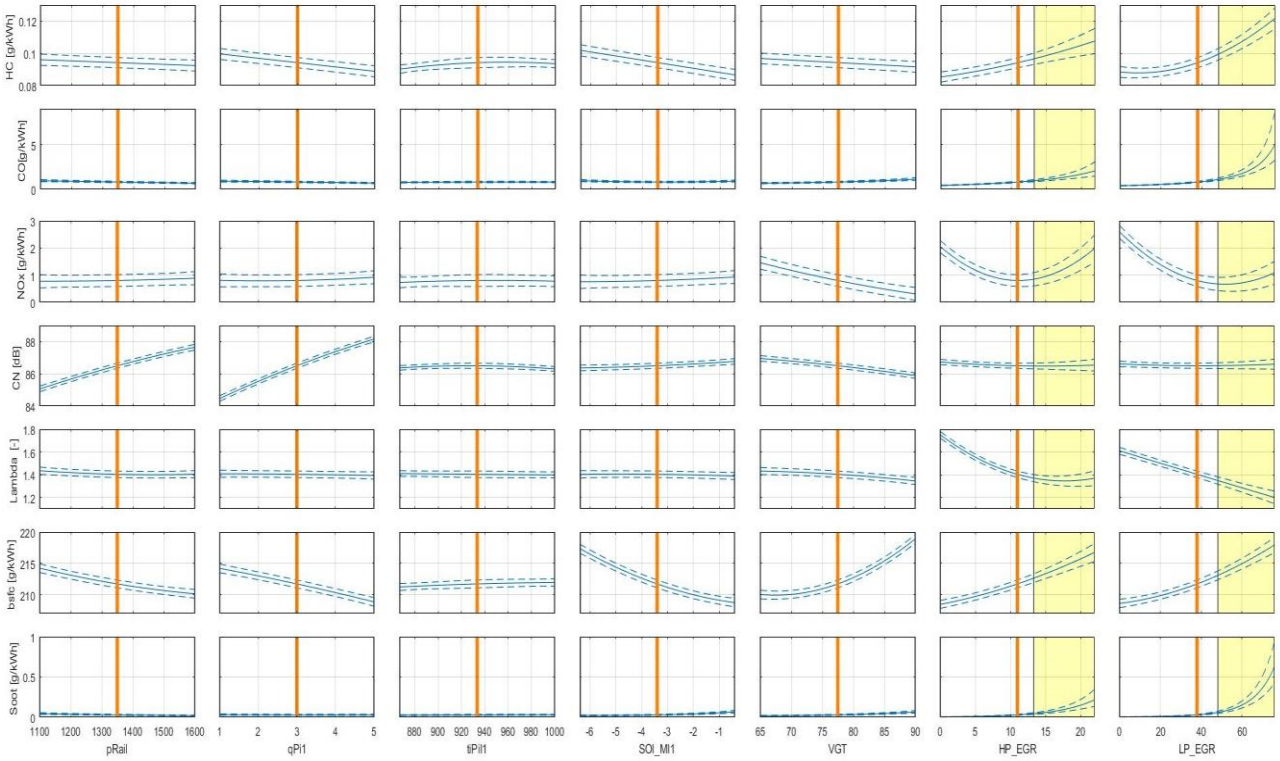

Figure 7.14 – Ressponse polynomial model MBC 2000x163 diesel.

7.3.3 2250x274

Response model statisics 2250 [rpm] x 274 [Nm] diesel								
Name	**Unit**	**Box-Cox**	**PRESS RMSE**	**RMSE**	**R^2**	**R^2adjusted**	**PRESS R^2**	**Test RMSE**
Lambda	[-]	1	0,039	0,037	0,964	0,959	0,952	0,032
CO	[g/kWh]	1	1,643	1,496	0,731	0,697	0,633	2,906
Soot	[g/kWh]	1	0,109	0,101	0,959	0,953	0,943	0,260
bsfc	[g/kWh]	1	1,661	1,498	0,952	0,944	0,931	3,450
CN	[dB]	1	0,242	0,215	0,990	0,988	0,985	0,418
NOx	[g/kWh]	1	0,374	0,337	0,975	0,971	0,964	3,661
HC	[g/kWh]	0	0,009	0,009	0,436	0,394	0,351	0,049

Table 7.6 – Statistical indicators polynomial model MBC 2250x274 diesel.

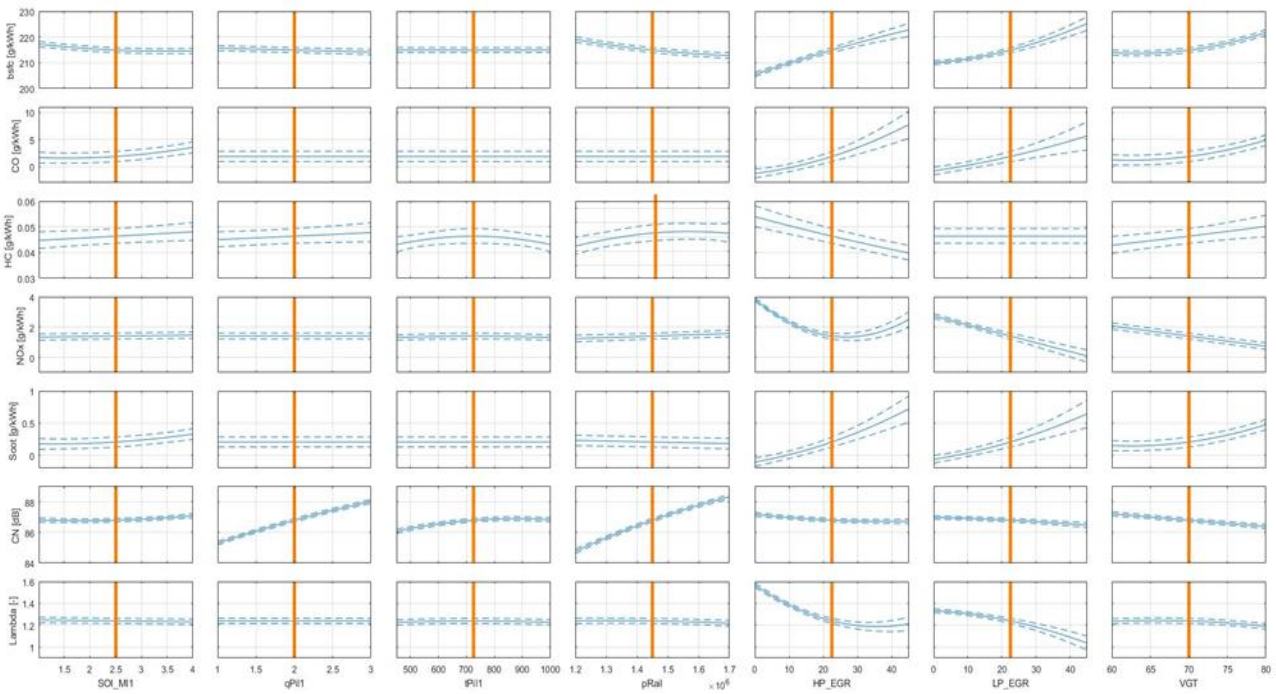

Figure 7.15 - Ressponse polynomial model MBC 2250x274 diesel.

Response model statisics 2250 [rpm] x 274 [Nm] HVO								
Name	**Unit**	**Box-Cox**	**PRESS RMSE**	**RMSE**	**R^2**	**R^2adjusted**	**PRESS R^2**	**Test RMSE**
Lambda	[-]	1	0,031	0,026	0,980	0,972	0,960	0,222
CO	[g/kWh]	1	0,184	0,161	0,844	0,813	0,753	0,254
Soot	[g/kWh]	1	0,013	0,011	0,843	0,813	0,767	0,020
bsfc	[g/kWh]	1	0,638	0,542	0,995	0,993	0,990	3,008
CN	[dB]	1	0,214	0,176	0,993	0,990	0,986	0,290
NOx	[g/kWh]	1	0,376	0,315	0,977	0,968	0,953	2,352
HC	[g/kWh]	1	0,004	0,003	0,917	0,884	0,828	0,008

Table 7.7 - Statistical indicators polynomial model MBC 2250x274 HVO.

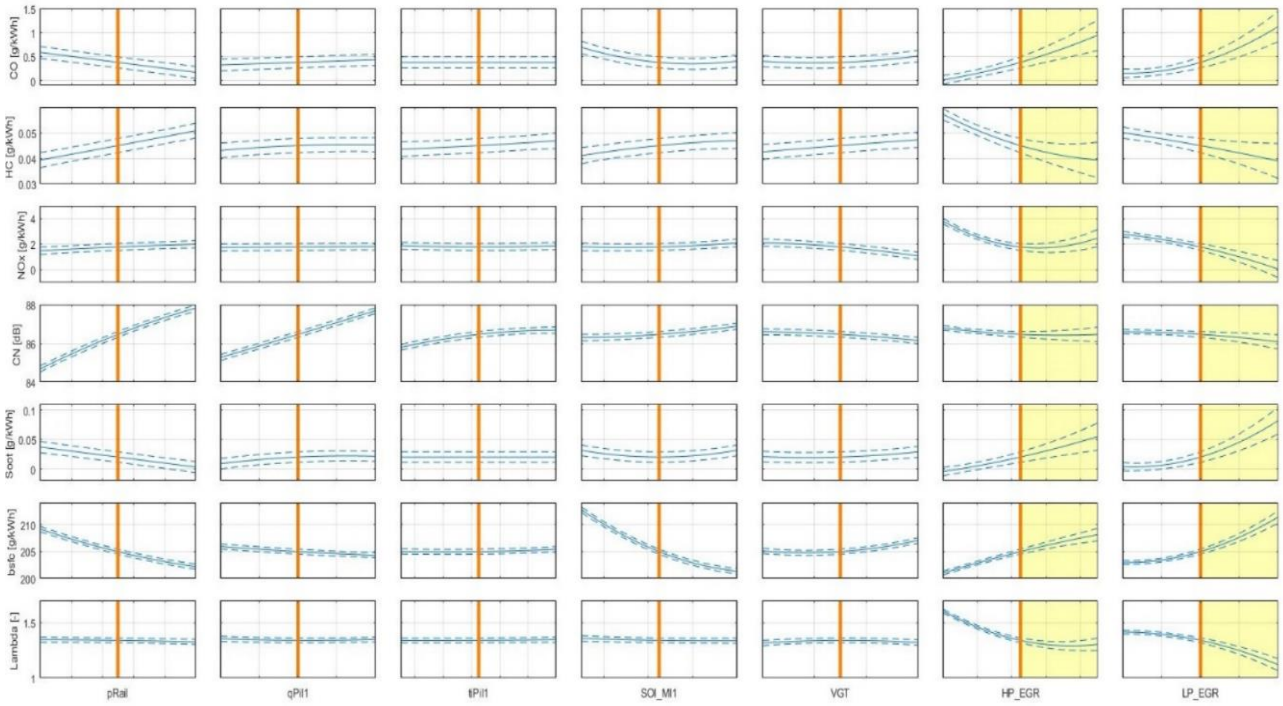

Figure 7.16 - Ressponse polynomial model MBC 2250x274 HVO.

7.4 ASCMO procedure for model fitting

The modelling approach used in ASCMO is different. It was decided to proceed by using the GP model since it is suggested by the ASCMO guide as the most functional method. The criticality faced by following this approach was to use the DoE data set built with the V-optimal method in MBC, which is not intended to be used with GP model. Fortunately, since we are dealing with the study of single engine operating points, this was not penalizing.

Figure 7.17 – Input and output selection ASCMO.

After that the model was created in ASCMO, in order to obtain results comparable with the one in MBC we followed the same approach for what concern the model fitting and improvement. To verify if the number of tests was adequate we used the function presents in ASCMO called LOO (leave one out figure 7.18).

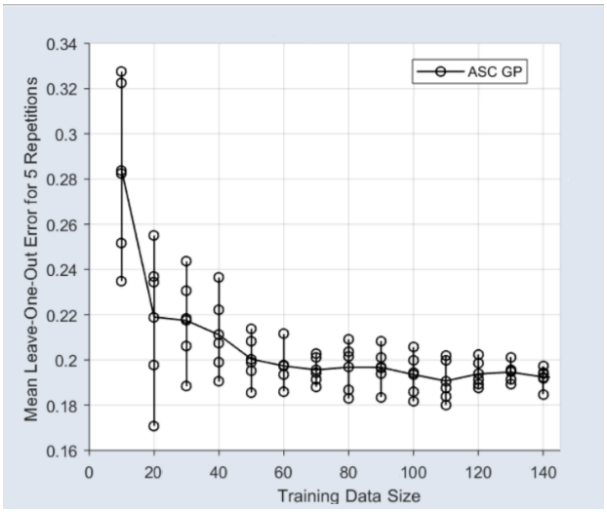

Figure 7.18 – LOO leave one out average RMSE vs model training data set size.

This function performs a number of iteration pre-imposed by the user for the interested number of the training data set size. Since we had sets made of 130 points (140 if we consider the repetition points), we want to see if a larger data set would benefit model quality, it was noted that an increase in the size of the data set would not bring any benefit for the majority of the outputs as the RMSE value tended to converge already to for a data set of around 100 training point, therefore the data set used seems reasonable. The first step to improve the model is the detection of the outliers. This procedure is performed by ASCMO, by verifying if the residual (error) of the predicted data is 3 or 4 times the RMSE.Is also possible to perform a visual check of the data using measured versus predicted graph and studentized residuals versus predicted value (figure 7.19 and figure). In ASCMO there was not the possibility to compute the Cook's distance since the GP model was adopted and the PRESS statistic is not computed in ASCMO. For what concern the selection of the Box-Cox transformation was preferred to leave the automatic choice to the software.

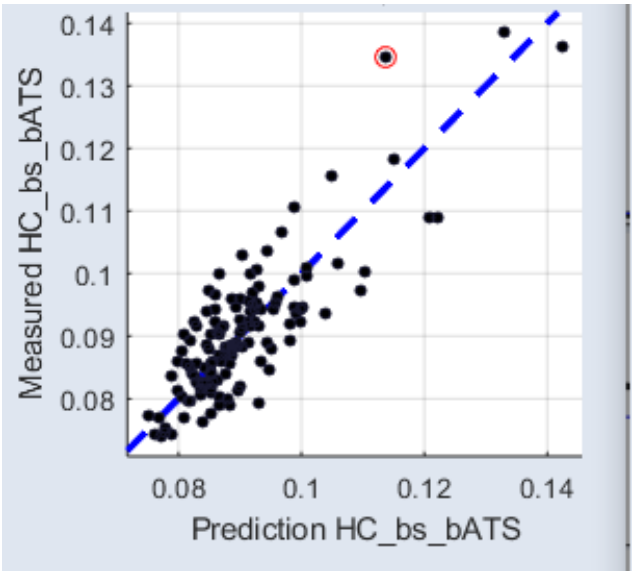

Figure 7.19 – Measured vs predicted graph.

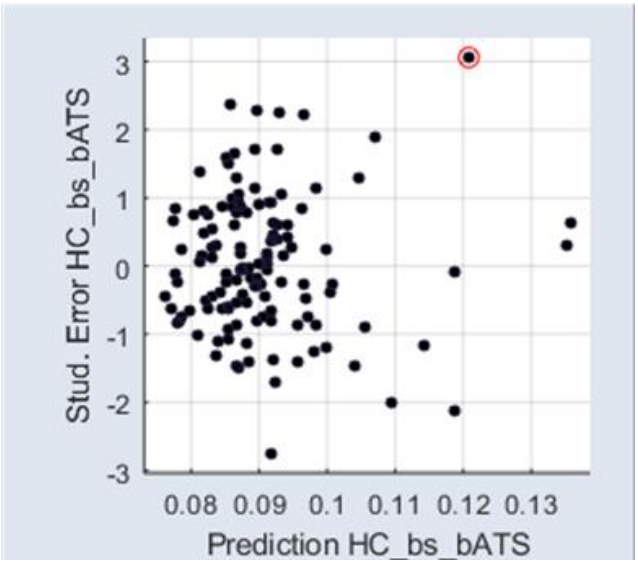

Figure 7.20 – Studentized residuals vs predicted graph.

7.4.1 1250x36

Even if the R^2 value of HC (table 7.8) seems better than the one obtained by polynomial model the response shows overfitting detectable in the HC response trend in figure 7.21 especially with respect the HP EGR input.

Response model statisics 1250x36 diesel				
Name	**Unit**	**RMSE**	**R^2**	**Test RMSE**
Lambda	[-]	0,114	0,900	0,148
CO	[g/kWh]	0,320	0,902	0,817
Soot	[g/kWh]	0,012	0,874	0,017
bsfc	[g/kWh]	1,777	0,812	4,548
CN	[dB]	0,204	0,978	0,778
NOx	[g/kWh]	0,330	0,897	0,331
HC	[g/kWh]	0,131	0,743	0,252

Table 7.8 - Statistical indicators GP model ASCMO 1250x36 diesel.

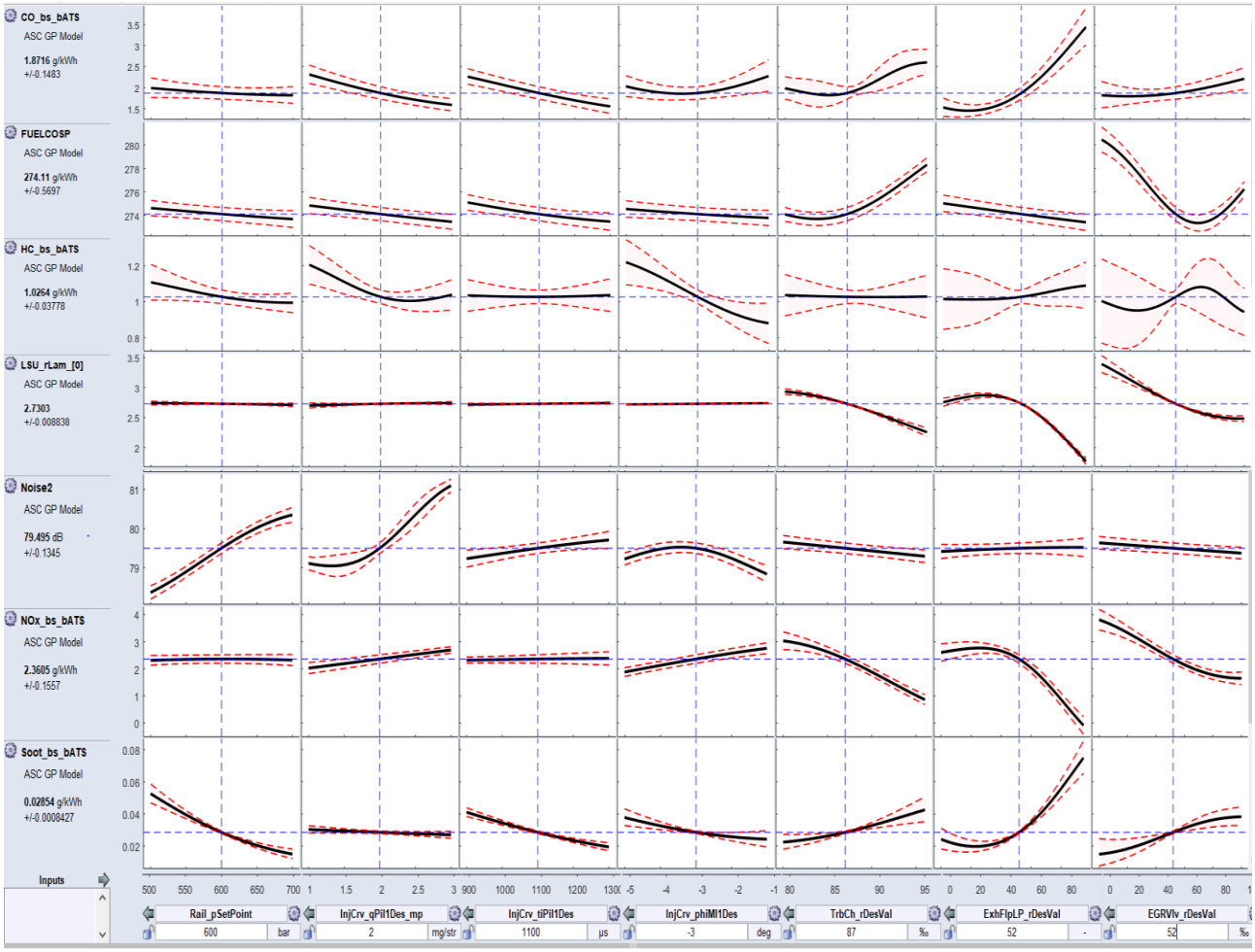

Figure 7.21 - Ressponse GP model ASCMO 1250x36 diesel.

Response model statisics 1250x36 HVO				
Name	**Unit**	**RMSE**	**R^2**	**Test RMSE**
Lambda	[-]	0,033	0,991	0,072
CO	[g/kWh]	0,159	0,937	0,335
Soot	[g/kWh]	0,006	0,922	0,007
bsfc	[g/kWh]	0,961	0,855	2,964
CN	[dB]	0,218	0,970	0,416
NOx	[g/kWh]	0,185	0,966	0,289
HC	[g/kWh]	0,026	0,917	0,044

Table 7.9 - Statistical indicators GP model ASCMO 1250x36 HVO.

there are no critical issues regarding the model created for the HVO for which shows for every output high quality.

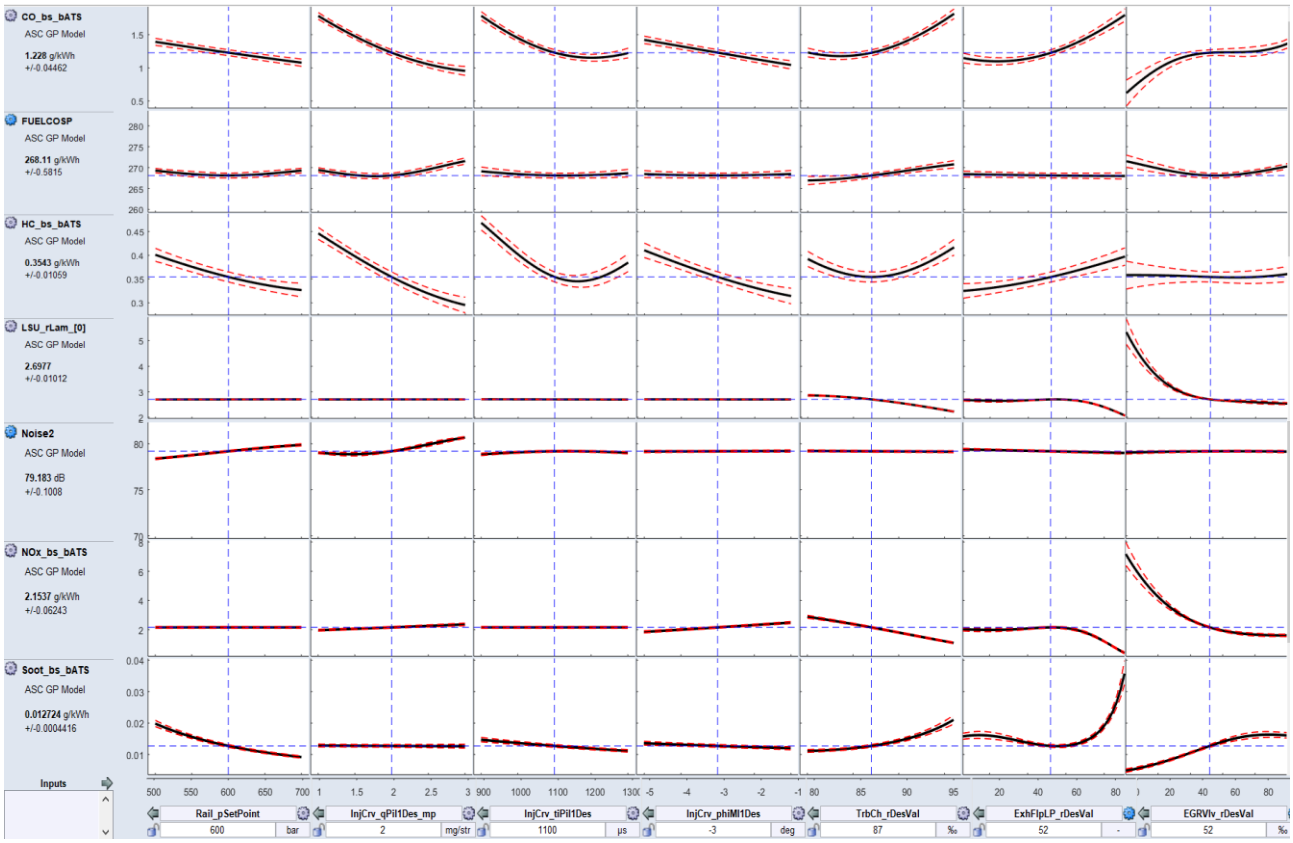

Figure 7.22 - Ressponse GP model ASCMO 1250x36 HVO.

7.4.2 2000x163

For this operating engine the resulting statistical indicator collected in table 7.10 and 7.11 shows high value of R^2 for every input and there is no overfitting both for HVO and diesel model.

Response model statisics 2000x163 diesel				
Name	**Unit**	**RMSE**	**R^2**	**Test RMSE**
Lambda	[-]	0,033	0,989	0,079
CO	[g/kWh]	0,192	0,846	0,259
Soot	[g/kWh]	0,041	0,843	0,026
bsfc	[g/kWh]	1,058	0,971	1,794
CN	[dB]	0,244	0,986	0,214
NOx	[g/kWh]	0,104	0,998	0,151
HC	[g/kWh]	0,007	0,809	0,018

Table 7.10 - Statistical indicators GP model ASCMO 2000x163 diesel.

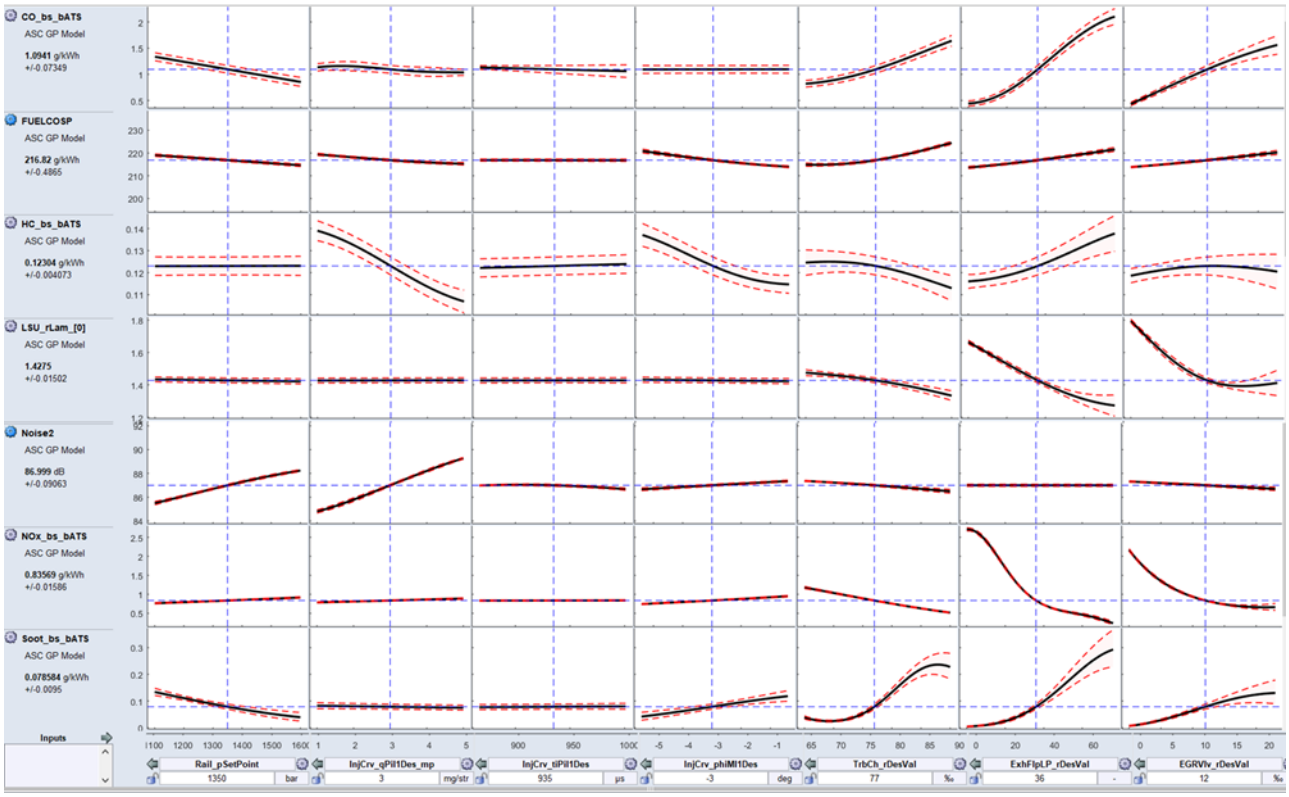

Figure 7.23 - Ressponse GP model ASCMO 2000x163 diesel.

Response model statisics 2000x163 HVO				
Name	**Unit**	**RMSE**	**R^2**	**Test RMSE**
Lambda	[-]	0,025	0,991	0,035
CO	[g/kWh]	0,113	0,955	0,264
Soot	[g/kWh]	0,011	0,973	0,014
bsfc	[g/kWh]	0,505	0,994	1,127
CN	[dB]	0,091	0,998	0,214
NOx	[g/kWh]	0,104	0,998	0,137
HC	[g/kWh]	0,004	0,879	0,011

Table 7.11- Statistical indicators GP model ASCMO 2000x163 HVO.

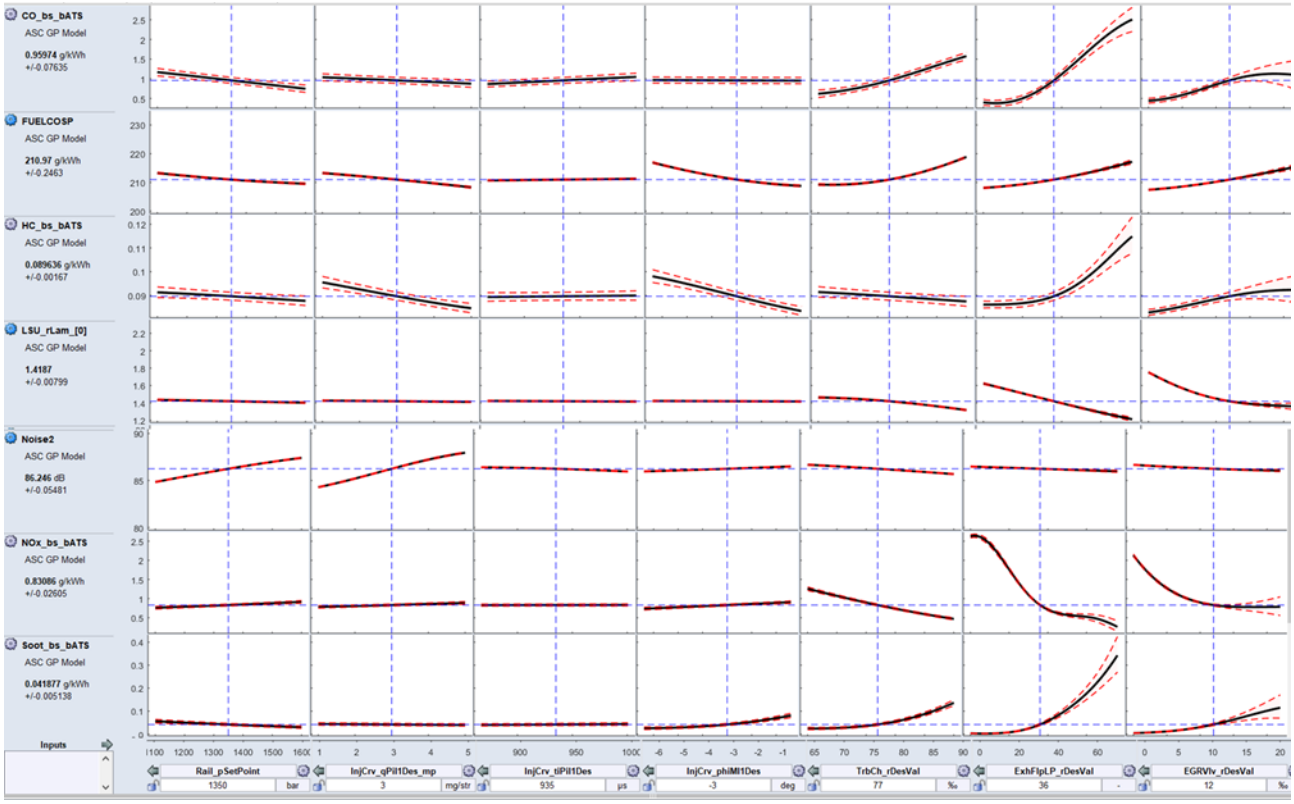

Figure 7.24 - Ressponse GP model ASCMO 2000x163 HVO.

7.4.3 2250x274

Response model statisics 2250x274 diesel				
Name	**Unit**	**RMSE**	**R^2**	**Test RMSE**
Lambda	[-]	0,021	0,987	0,037
CO	[g/kWh]	0,429	0,977	0,146
Soot	[g/kWh]	0,049	0,960	0,023
bsfc	[g/kWh]	0,760	0,987	1,333
CN	[dB]	0,126	0,998	0,214
NOx	[g/kWh]	0,104	0,996	0,112
HC	[g/kWh]	0,005	0,805	0,008

Table 7.12 - Statistical indicators GP model ASCMO 2250x163 diesel

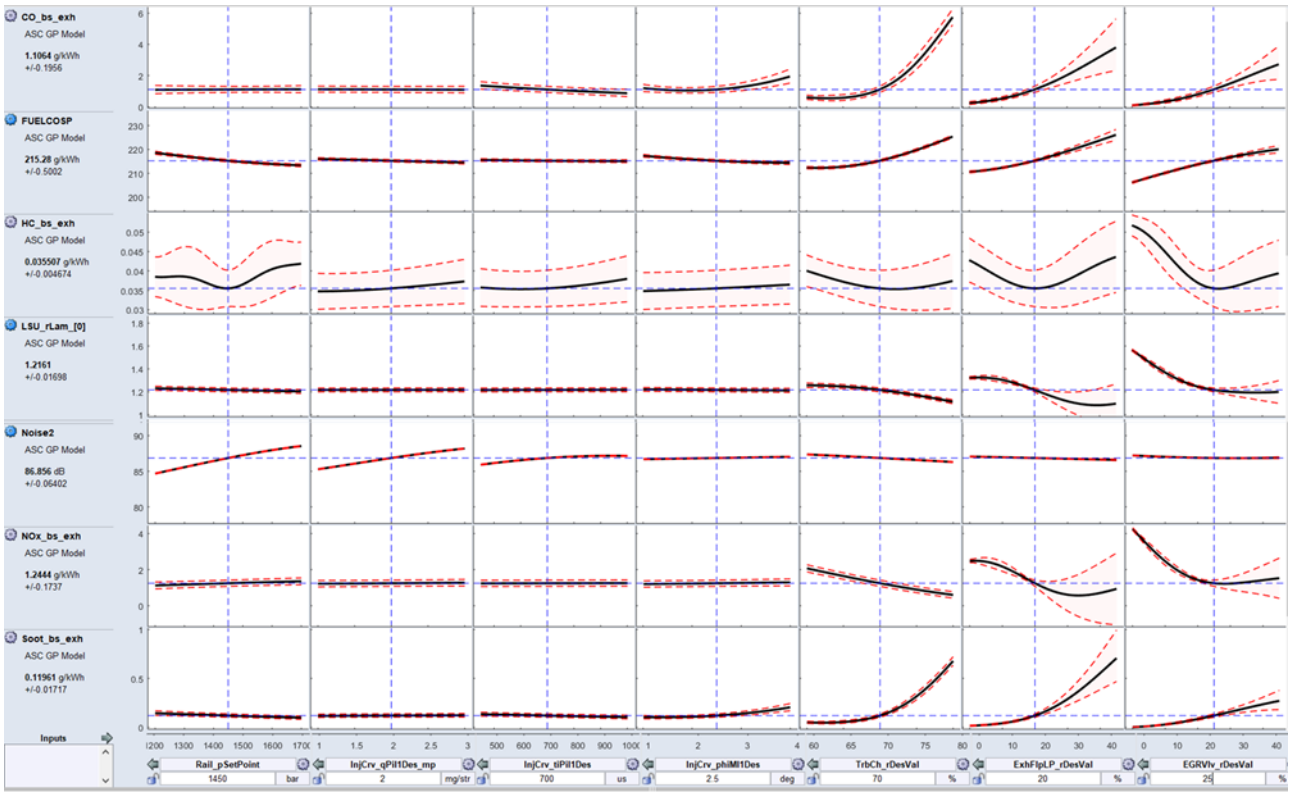

Figure 7.25 - Ressponse GP model ASCMO 2250x163 diesel.

Response model statisics 2250x274 HVO				
Name	**Unit**	**RMSE**	**R^2**	**Test RMSE**
Lambda	[-]	0,019	0,985	0,094
CO	[g/kWh]	0,094	0,943	0,123
Soot	[g/kWh]	0,011	0,810	0,009
bsfc	[g/kWh]	0,904	0,987	2,510
CN	[dB]	0,293	0,975	0,126
NOx	[g/kWh]	0,179	0,989	0,491
HC	[g/kWh]	0,003	0,902	0,005

Table 7.13- Statistical indicators GP model ASCMO 2250x163 HVO.

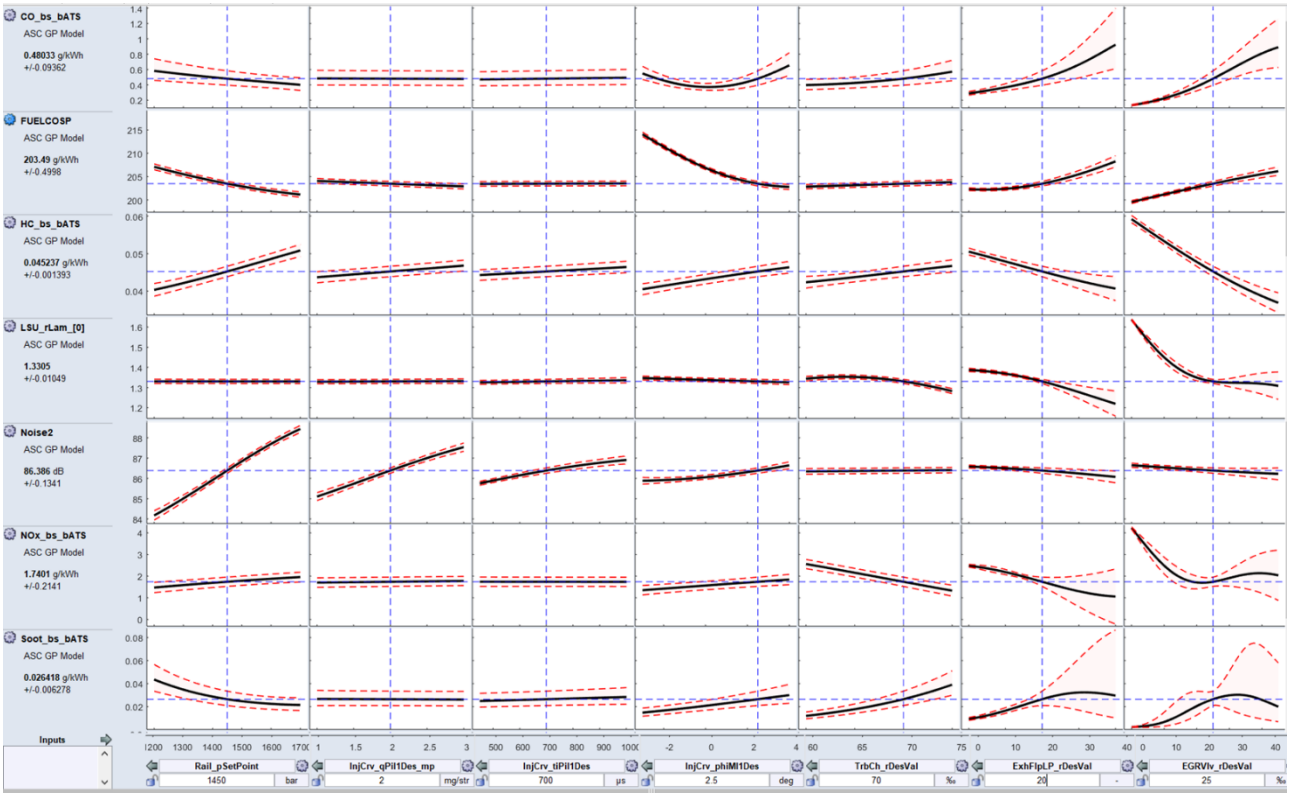

Figure 7.26 - Ressponse GP model ASCMO 2250x163 HVO.

7.5 Optimization results

On the basis of the created models, the optimal calibrations were found. To achieve this objective, firstly the limits of the pollutant emissions under which we were interested to stay were established. The starting point for determining these limits was the baseline calibration results already available for engine layouts similar to the one under study. On the basis of these previous calibrations a series of constraints have been proposed to be respected for each engine working point studied. These constraints represented the limitations for optimizations found with MATLAB toolbox CAGE and ASCMO, respectively. The limits are proposed below.

Objective	constraints							optimization n°
	bsfc [g/kWh]	CO [g/kWh]	NOx [g/kW]	HC [g/kWh]	Soot [g/kWh]	CN [dB]	EGR limit	
	285		0,95	0,75	0,08		yes	1
	285		0,95	0,75			yes	2
	285		0,95	1,5	0,08			3
min CO	285		0,95	1,5				4
	285	3,5	2		0,85		yes	5
min HC	285	3,5	2		0,85			6
	285	3,5		0,75	0,03		yes	7
	285	3,5		0,75			yes	8
	285	3,5		0,75	0,03			9
min NOx	285	3,5		0,75				10
min bsfc		3,5	0,95	0,75	0,08		yes	11
min CN		3,5	1,5	0,75	0,03		yes	12

Table 7.14 - 1250x36 optimization criterion and constraints

Objective	constraints							optimization n°
	bsfc [g/kWh]	CO [g/kWh]	NOx [g/kW]	HC [g/kWh]	Soot [g/kWh]	CN [dB]	EGR limit	
	216	0,9			0,07		yes	1
	221	0,92			0,2		yes	2
	210	0,9			0,07	88	yes	3
min Nox	217,5	0,563		0,122				4
	216	0,9	0,987				yes	5
	221	0,9	0,4				yes	6
min Soot	210	0,9	0,4					7
	216		0,98		0,07		yes	8
	216		0,6		0,07		yes	9
min CO	212		0,6		0,07		yes	10
	216	0,9	0,6		0,07		yes	11
	216	0,9	0,6		0,07		yes	12
min CN	212	0,9	0,6		0,7		yes	13
		0,9	0,98		0,07		yes	14
min bsfc		0,9	0,6		0,07	88		15

Table 7.15 – 2000x163 optimization criterion and constraints

Objective	constraints							optimization n°
	bsfc [g/kWh]	CO [g/kWh]	NOx [g/kW]	HC [g/kWh]	Soot [g/kWh]	CN [dB]	EGR limit	
	210				0,01		yes	1
					0,004		yes	2
					0,05		yes	3
	212						yes	5
					0,05			6
min Nox	212							7
			2,7				yes	8
min Soot	210		2				yes	9
min CN	210		2,7		0,05			10
			2,7					11
			2					12
			2			87		13
min bsfc			1			88		14

Table 7.16 – 2250x274 optimization criterion and constraints

In the tables from 7.14 to 7.16 all the criteria used to carry out the optimization are reported. The objective was the output which was intended to be minimized while the constraints were the limits that we impose to the solution that both the software must respect. The series of optimization criteria were found by trying various combinations of limits that led to the achievement of the imposed objective by both ASCMO and CAGE. It was taken into account that the 3 optimized operating points represent 3 different load conditions.

7.5.1 Results comparison

The optimization obtained from ASCMO and CAGE were compared. This approach was intended to test how much the results of both the optimizations obtained differ one with respect to the other. The final step was to verify these obtained optimizations experimentally on the test bench. The comparison will be done first between optimizations obtained with each software by cross comparison. The differences will be calculated with percentages obtained with the expression 7.1:

$$\% = \frac{ASCMO - CAGE}{CAGE} \tag{7.1}$$

it can be seen in figures 7.25 and 7.26, that takes into account the optimization number 10 in table 7.14, how there is a great difference between the calibration of the HP EGR actuator, especially as regards the diesel, seeing an increase in favour of ASCMO. This could be related to the fact that ASCMO did not takes into account the limit in the EGR actuation domain, so to face the minimization of the NOx, which was the goal of this optimization, tends to increase the amounts of the high pressure EGR. A direct consequence of this is the difference in the prediction of NOx for conventional diesel that results lower for the ASCMO model figure 7.29 and 7.30.

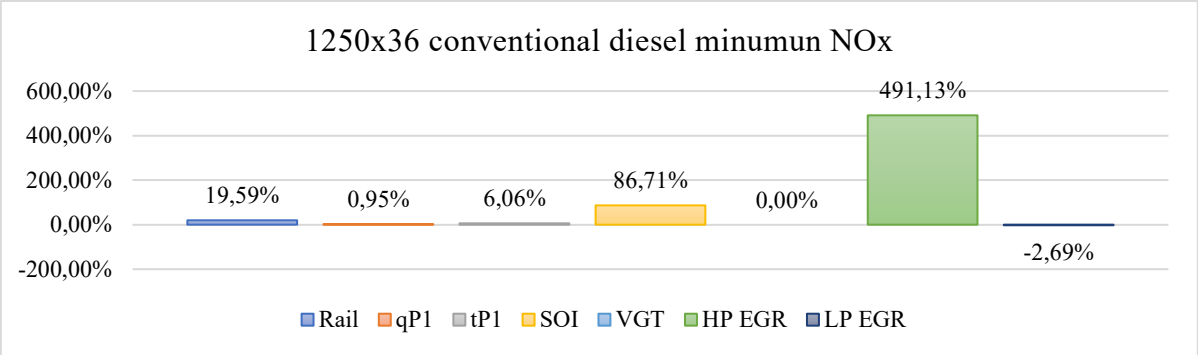

Figure 7.27 – 1250x36 diesel optimization number 10 table 7.14 input calibration.

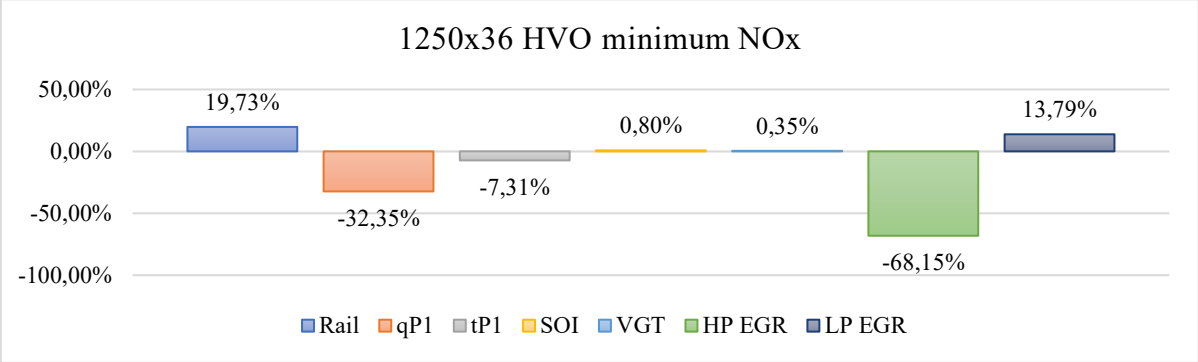

Figure 7.28 - – 1250x36 HVO optimization number 10 table 7.14 input calibration.

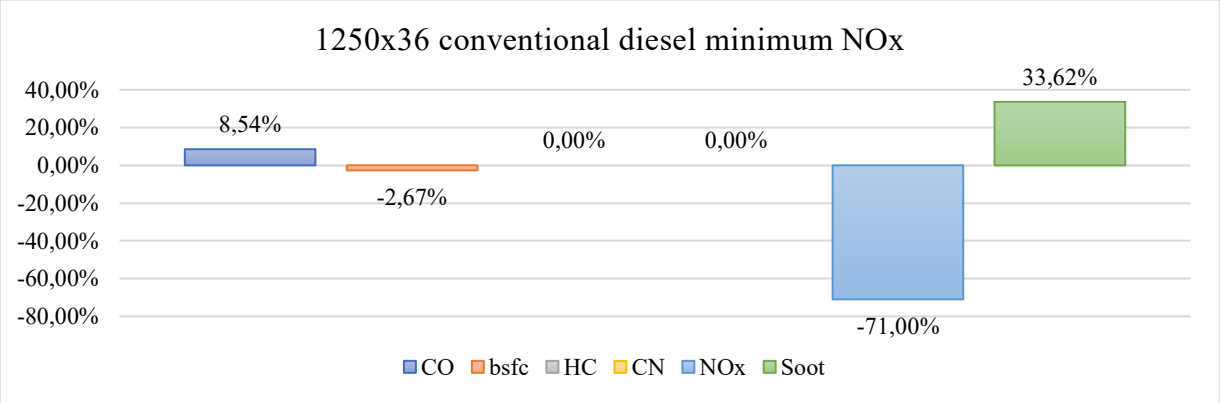

Figure 7.29 - 1250x36 diesel optimization number 10 table 7.14 output results.

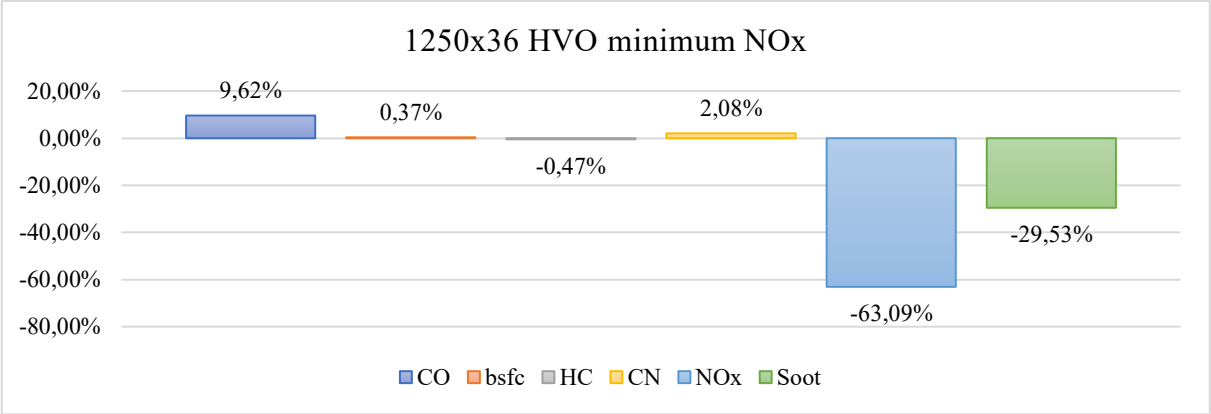

Figure 7.30 - 1250x36 HVO optimization number 10 table 7.14 output results.

The experimental validation of the calibrations found, was carried out only for the results obtained with CAGE. The difference in percentage between experimental and model results is obtained with the expression 7.2.

$$\% = \frac{experimental - CAGE}{CAGE} \tag{7.2}$$

Below are reported the optimization found that gave results closer to the experimental ones.

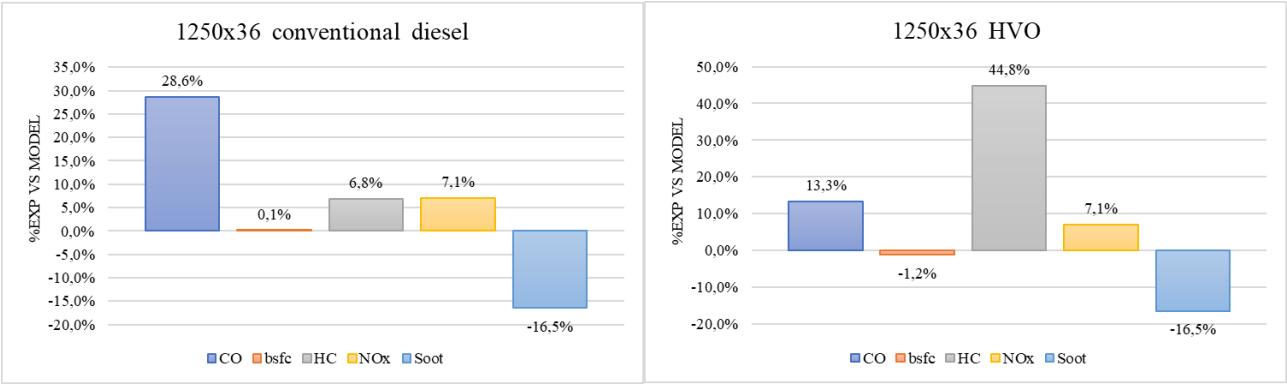

Figure 7.31 – optimization number 7 for diesel and number 1 for HVO of table 7.14.

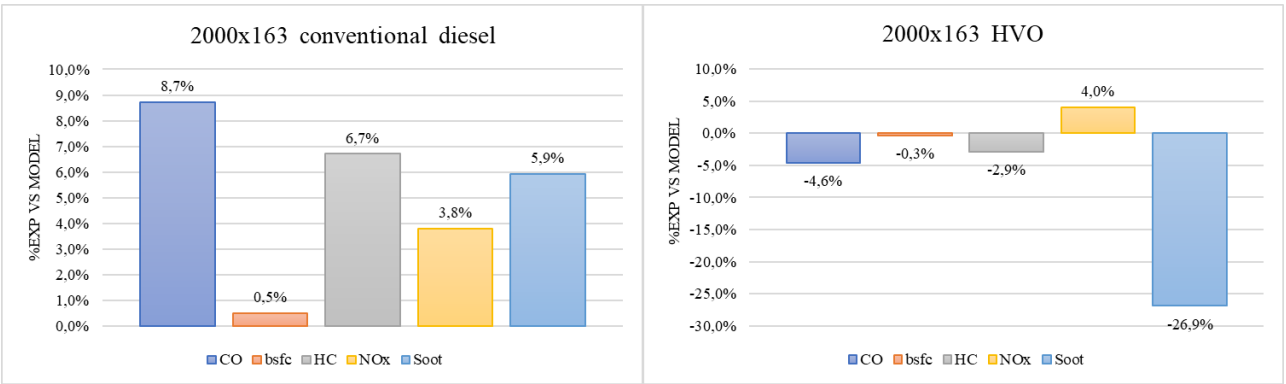

Figure 7.32 - optimization number 8 for diesel and number 8 for HVO of table 7.15

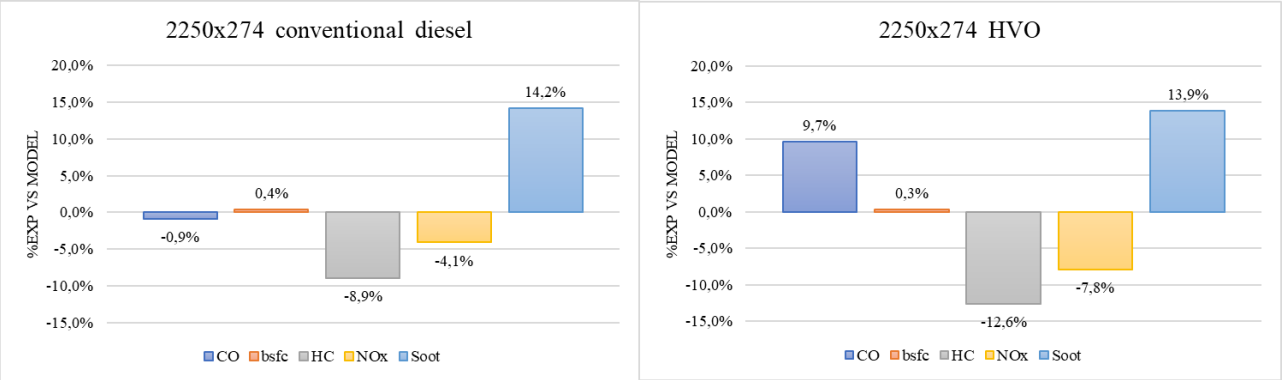

Figure 7.33 - optimization number 6 for diesel and number 2 for HVO of table 7.16

It is worth highlighting by looking at the figures 7.31 and 7.32 and 7.33 how the models created tend to predict experimental data well. However, it can be seen that there is a large difference in percentage as regards the soot for HVO of the points 1250x36 and 2000x163, the HC of 1250x36 HVO and CO of 1250x36 diesel, of which the absolute values are still lower than base calibration both for the experimental and model results. One result that comes out by analysing the resulting calibration is that the pollutant emissions decrease if the engine run on HVO with respect both the optimal and base calibration of diesel. In particular the results depend on the engine working point for the low load 1250 [rpm] x 36 [Nm] where the emissions of CO are relevant, due to their high presence since the low in-cylinder temperature, there is a relevant reduction of CO for HVO with respect conventional diesel. In figure 7.34 the optimization that minimizes the CO for both fuels is represented.

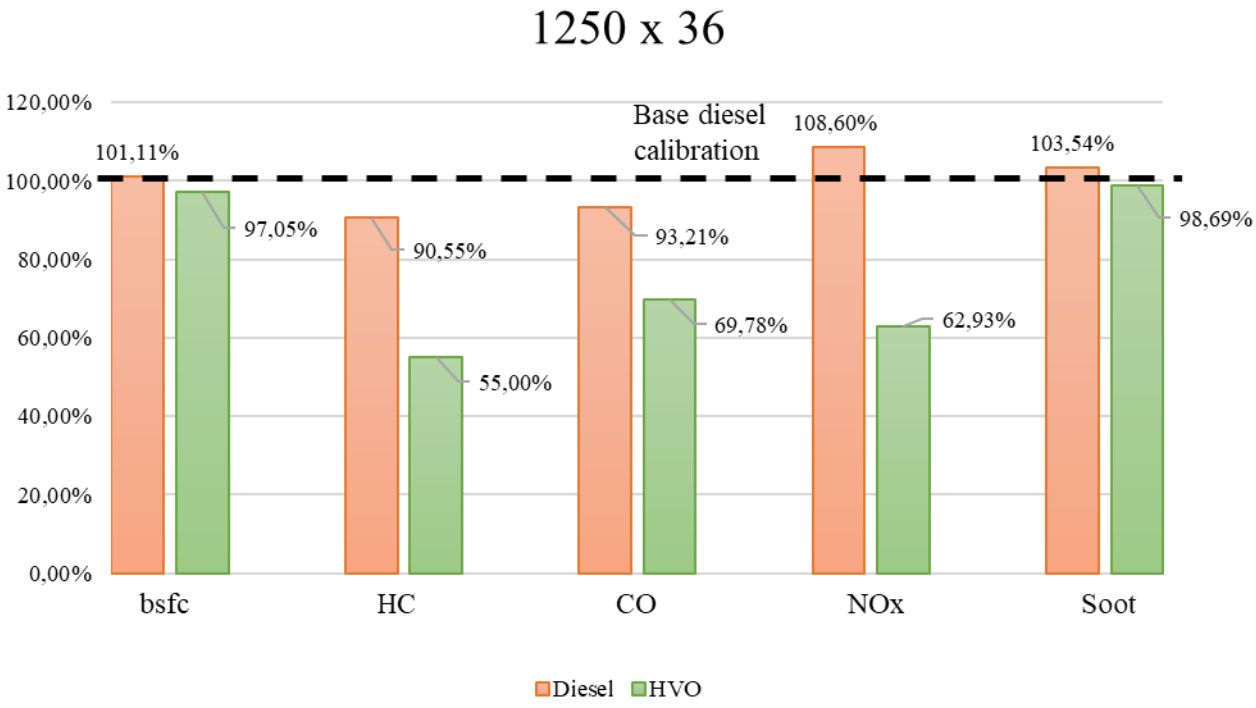

Figure 7.34 - Point 1250 [rpm] x 36 [Nm] optimal calibration for conventional diesel and HVO vs Base diesel calibration

At higher load the CO and HC emissions are less relevant than NOx emissions, since the cylinder temperature higher than the one at low load helps their oxidations. So, the aim of the optimization for the points 2000x163 and 2250x274 was the NOx reduction also taking into account the NOx soot trade off. It can be seen that using

HVO there is a significant reduction in soot (figure 7.35, figure 7.36). This trend can be explained by the absence of aromatics in the HVO.

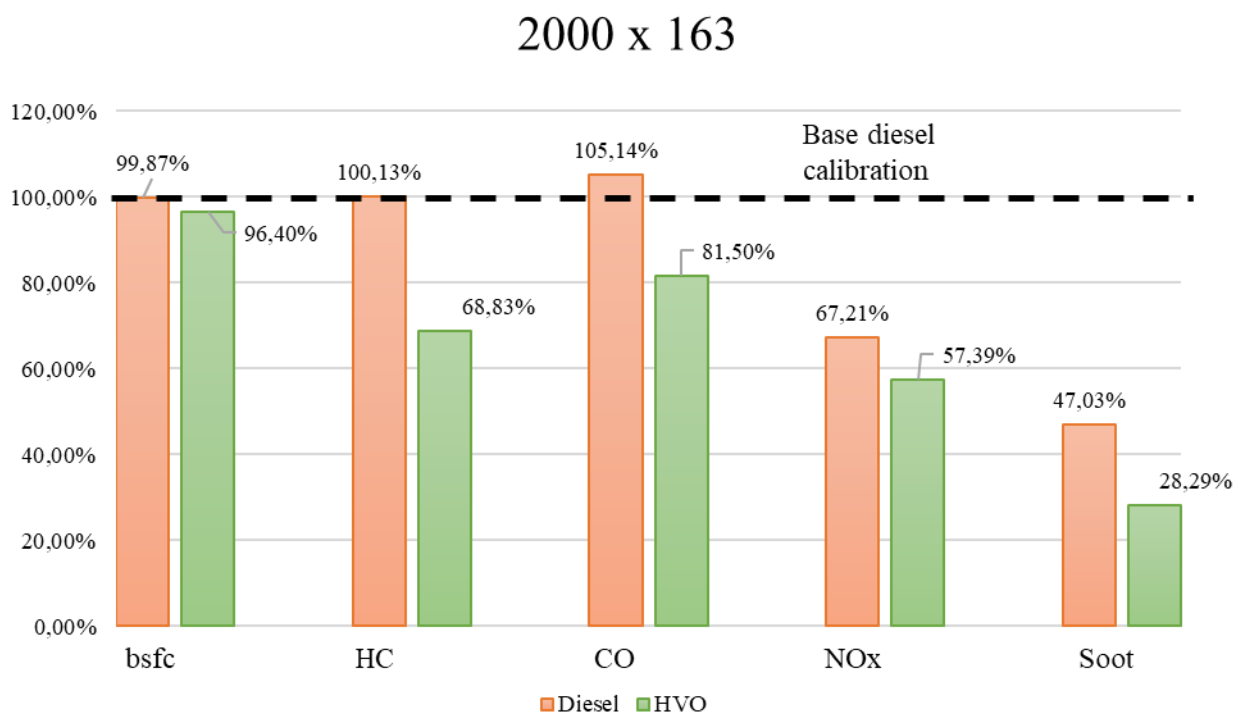

Figure 7.35 - Point 2000 [rpm] x 163 [Nm] optimal calibration for conventional diesel and HVO vs Base diesel calibration.

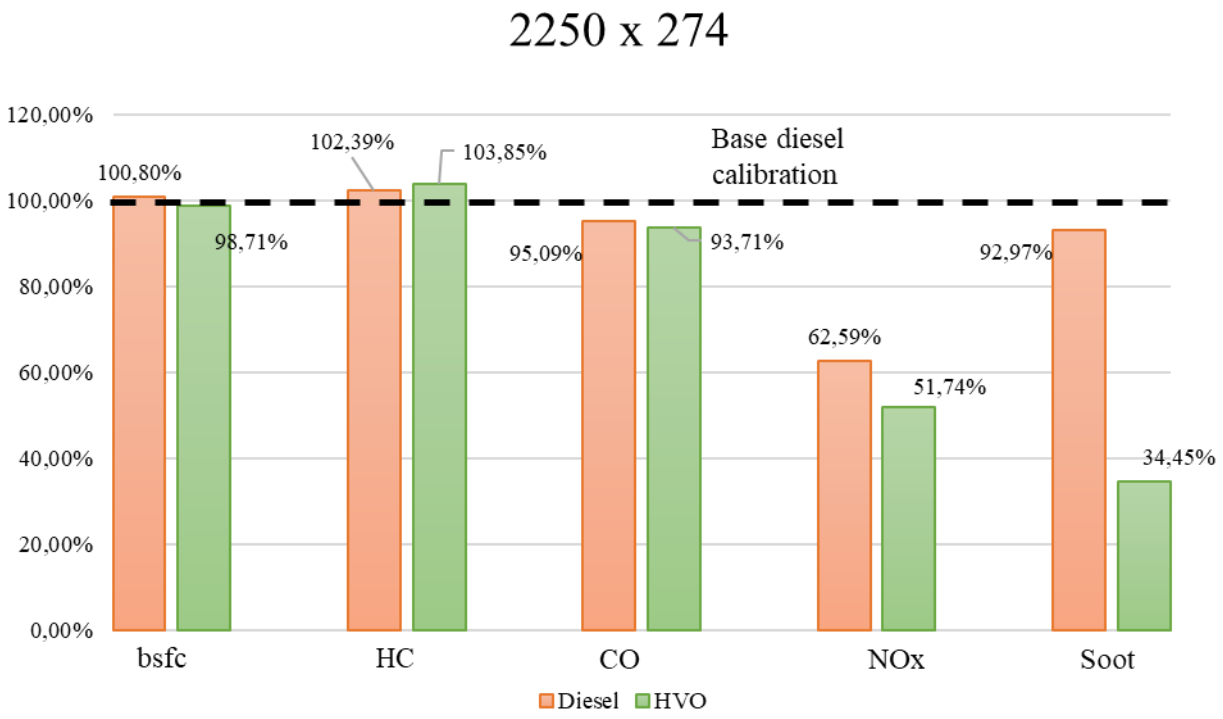

Figure 7.36 - Point 2250 [rpm] x 274 [Nm] optimal calibration for conventional diesel and HVO vs Base diesel calibration.

8. Conclusions

The objective of the work was to create a robust calibration of a light duty engine compliant with the euro 6 legislation to further reduce the main pollutant emissions, consumption and combustion noise. The tests were conducted by running the engine with 2 type of fuels HVO and B7 EN590. The procedure followed to minimize this time spending procedure was based on DoE theory. The DoE variation list was created by means of the MATLAB toolbox MBC. The scheduled tests results, then were manipulated with MBC and ASCMO in order to create the regression models adopted to perform optimizations of the calibrations. The calibrations regarded in particular three engine points representing three load condition of the engine low medium and high. We can deduce how the strategy of adopting the DoE is advantageous to carry out the calibration of an engine in order to save time. The use of the MATLAB toolbox MBC is adequate in the creation of models which, after a careful optimization, proved to be able to adequately predict the results obtained experimentally. For what concern the tool ASCMO static it was possible to notice during its utilization, a greater simplicity compared to MBC and the ability to create high quality models that do not fall into overfitting. Furthermore, it was possible to see that although a different method was adopted to create the empirical models, the calibrations found following the same optimization criteria were close to those obtained with MBC. Throughout the study it was possible to state that the use of HVO could represents an alternative to conventional diesel. The study could be completed by experimenting with the use of the so-called global model that which, unlike the method used in this work, allows a study of the engine under analysis on the entire engine map, thus guaranteeing the possibility of creating more robust calibrations.

References

[1] F. Millo, *Engine emissions control*, MSc in Automotive Engineering, Politecnico di Torino.

[2] J. Ashwin, B. Ashok, *An interdisciplinary review on calibration strategies of engine management system for diverse alternative fuels in IC engine applications*.

[3] J.B. Heywood, *Internal combustion engine fundamentals*, second edition. New York: McGraw-Hill, 2018.

[4] J.E. Dec, *A Conceptual Model of DI Diesel Combustion Based on Laser-sheet Imaging*. SAE International, 1997.

[5] G.P. Merker, C. Schwarz, R. Teichmann. *Combustion Engines Development Mixture Formation, Combustion, Emissions and Simulation.* Springer-Verlag Berlin Heidelberg 2012.

[6] C.R. Ferguson, A.T. Kirkpatrick, *Internal Combustion Engines: Applied Thermosciences,* third edition. John Wiley and Sons Ltd, 2016

[7] S. D'Ambrosio, *Combustion engines and their application to vehicle,* MSc in Automotive Engineering, Politecnico di Torino

[8] D. C. Montgomery. *Design and analysis of experiments,* eighth edition, 2012.

[9] T.W. Simpson, J.D. Poplinski, P.N. Koch, J.K. Allen. *Metamodels for computer-based engineering design: survey and recommendations*. Engineering with Computers 2001, 17(2):129–150.

[10] M. Cavazzuti, *Optimization Methods: From Theory to Design Scientific and Technological Aspects in Mechanics*, Springer-Verlag Berlin Heidelberg, 2013.

[11] R. T. Johnson, D. C. Montgomery, B. A. Jones, *An Expository Paper on Optimal Design*, Article in Quality Engineering 2011 DOI: 10.1080/08982112.2011.576203.

[12] D.C. Montgomery, E.A. Peck, G.G.Vining, *Introduction to Linear Regression Analysis,* fifth edition, Wiley,2012

[13] D.C. Montgomery, G.C. Runger, N. Faris Hubele, *Engineering statistics,* fifth edition.

[14] K. Takeuchi, *International Encyclopedia of the Social & Behavioral Sciences*, 2001.

[15] C.E. Rasmussen & C.K.I. Williams, *Gaussian Processes for Machine Learning*, the MIT Press, 2006.

[16] Matlab documentation, *Guidelines for Selecting the Best Model Fit.*

[17] AVL documentation, *http://www.avl.co.jp/service/pdf/Product%20Sheet%20DynoExact_e.pdf*

[18] Kistler documentation, url:https://www.kistler.com/en/products/components/pressuresensors/?pfvmetrics=metric

[19] M. Paulweber, K. Lebert *Powertrain Instrumentation and Test Systems: Development – Hybridization – Electrification,* Springer 2016.

[20] S. Gluck, C. Glenn, T. Logan, B. Vu, M. Walsh, P. Williams *Evaluation of NOx Flue Gas Analyzers for Accuracy and Their Applicability for Low-Concentration Measurements*, Article in Journal of the Air & Waste Management Association (1995) · July 2003.

[21] A. J. Martyr, M. A. Plint *Engine Testing: The Design, Building, Modification and Use of Powertrain Test Facilities*, fourth edition, Butterworth-Heinemann ,2012.

[22] R. Viskup (February 11th 2020). *Comparison of Different Techniques for Measurement of Soot and Particulate Matter Emissions from Diesel Engine* Introduction to Diesel Emissions, Richard Viskup, IntechOpen, DOI: 10.5772/intechopen.91186. Available from: https://www.intechopen.com/chapters/71028

[23] G. Zamboni, M. Capobianco *Experimental study on the effects of HP and LP EGR in an automotive turbocharged diesel engine.* Applied Energy – Elsevier, 2012.

[24] Matlab documentation*, Stepwise regression*.